Shi et al. ; revision of resubmitted (JPHYSIOL/2004/075051)

(Previous Ms No.: JPHYSIOL/2003/058990)

Multiple regulation by calcium of murine homologues of transient receptor potential proteins TRPC6 and TRPC7 expressed in HEK293 cell

Juan Shi [1, 4], Emiko Mori [2], Yasuo Mori [2], Masayuki Mori [3], Jishuo Li[4], Yushi Ito[1] and Ryuji Inoue[1,*]

[1]Department of Pharmacology, Graduate School of Medical Sciences, Kyushu University, Fukuoka 812-8582, Japan; [2]Laboratory of Molecular Biology, Department of Synthetic Chemistry & Biological Chemistry, Graduate School of Engineering, Kyoto University, Kyoto 606-8510, Japan.; [3]National Institute for Physiological Sciences, Okazaki 444-8585, Aichi, Japan; [4]Department of Anatomy, the Fourth Military Medical University, Xi'an 710032, China

*Corresponding author: Ryuji Inoue at the above address

Tel.: +81-92-642-6076

Fax: +81-92-642-6079

E-mail: inouery@pharmaco.med.kyushu-u.ac.jp

Running title: Ca^{2+}/calmodulin regulation of TRPC6 and TRPC7 channels

Key words: Ca^{2+}, calmodulin, canonical TRP channel, receptor-operated Ca^{2+} entry

Abstract

We investigated, by using the patch clamp technique, Ca^{2+}-mediated regulation of heterologously expressed TRPC6 and TRPC7 proteins in HEK293 cells, two closely related homologues of transient receptor potential (TRP) family and molecular candidates for native receptor-operated Ca^{2+} entry channels. With nystatin-perforated recording, the magnitude and time courses of activation and inactivation of carbachol (CCh; 100μM)-activated TRPC6 currents (I_{TRPC6}) were enhanced and accelerated respectively by extracellular Ca^{2+} (Ca^{2+}_o) whether it was continuously present or applied after receptor stimulation. In contrast, Ca^{2+}_o solely inhibited TRPC7 currents (I_{TRPC7}). Vigorous buffering of intracellular Ca^{2+} (Ca^{2+}_i) under conventional whole-cell clamp abolished the slow potentiating (i.e. accelerated activation) and inactivating effects of Ca^{2+}_o, disclosing fast potentiation (EC_{50}:~0.4mM) and inhibition (IC_{50}:~4mM) of I_{TRPC6} and fast inhibition (IC_{50}:~0.4mM) of I_{TRPC7}. This inhibition of I_{TRPC6} and I_{TRPC7} seems associated with voltage-dependent reductions of unitary conductance and open probability at the single channel level, whereas the potentiation of I_{TRPC6} showed little voltage-dependence and was mimicked by Sr^{2+} but not Ba^{2+}. The activation process of I_{TRPC6} or its acceleration by Ca^{2+}_o likely involve phosphorylation by calmodulin (CaM)-dependent kinase II (CaMKII), as pretreatment with calmidazolium (3μM), coexpression of Ca^{2+}-insesentive mutant CaM, and intracellular perfusion of nonhydrolyzable ATP analogue AMP-PNP and a CaMKII-specific inhibitory peptide all effectively prevented channel activation. However, this was not observed for TRPC7. Instead, single CCh-activated TRPC7 channel activities were concentration-dependently

suppressed by nanomolar Ca^{2+}_i via CaM and conversely enhanced by IP_3. In addition, the inactivation time course of I_{TRPC6} was significantly retarded by pharmacological inhibition of protein kinase C (PKC). These results collectively suggest that TRPC6 and 7 channels are multiply regulated by Ca^{2+} from both sides of the membrane through differential Ca^{2+}/CaM-dependent and -independent mechanisms.

Introduction

Ca^{2+}-dependent regulation is a ubiquitous mechanism by which the activity of various types of Ca^{2+} permeable cation channels is finely tuned (Levitan, 1999; Saimi and Kung, 2002). Examples are not restricted to small conductance Ca^{2+}-activated K^+ channels, cyclic nucleotide-gated cation channel, NMDA receptor, ryanodine/inositol 1,4,5,-trisphospate (IP_3) receptors and L-, P/Q type voltage-dependent Ca^{2+} channels, but also include a variety of native receptor-operated cation (ROC) channels with less well elucidated properties (e.g. Siemen, 1993) and their molecular candidates, the mammalian homologues of *Drosophila* transient receptor potential (TRP/TRPL) protein (Montell, 2001; Clapham *et al*., 2001; Minke and Cook, 2002).

In photoreceptor cells of the wild-type *Drosophila*'s eye, it was originally found that light-induced currents which reflect the opening of TRP and TRPL channels are dually modulated by photolytically released Ca^{2+} with facilitation and inactivation in rising and plateau phases of the response respectively (Hardie *et al*., 1995). Later, a similar reciprocal regulation by Ca^{2+} was also found for the canonical members of the TRP superfamily (TRPC). Earlier studies demonstrated that maneuvers to increase $Ca^{2+}{}_i$ concentration ($[Ca^{2+}]_i$) such as application of ionomycin and direct Ca^{2+} infusion into the cell enhanced the activities of heterologously expressed TRPC3 channels (Zitt *et al*., 1997), while sustained elevation in $[Ca^{2+}]_i$ by use of Ca^{2+}/EGTA or BAPTA failed to stimulate or even inhibited them (Zitt *et al.*, 1997; Kamouchi *et al*., 1999). It has subsequently been shown that a CaM binding site (CIRB), which also exhibits binding affinity for IP_3 receptor (IP_3R), is present on the carboxy tail of TRPC3 channels (Zhang

et al., 2001), and highly homologous CaM binding sites to this are identified in all other members of TRPC family (Tang et al., 2001). It has experimentally been shown that application of CaM antagonists or IP_3R peptides relieves the tonic inhibitory effects of CaM via CIRB thereby increasing the basal TRPC3 channel activities. This observation has been interpreted to represent the molecular mechanism underlying store depletion-activated Ca^{2+} entry (SOC) during receptor stimulation (Kiselyov *et al.*, 1998; Boulay *et al*., 1999; Zhang *et al*., 2001). However, there is also good evidence to suggest that members of TRPC3/6/7 subfamily are activated by diacylglycerol in a store-independent fashion (e.g. Hofmann *et al.*, 1999; Trebak *et al.*, 2003). Inhibitory actions of CaM have also been suggested for TRPC4 (Tang *et al.*, 2001) and TRPC1 (Singh *et al.*, 2002; Vaca and Sampieri, 2002). In the latter, the role of CaM has been assigned to Ca^{2+}-dependent feedback inhibition of endogenous SOC via a C-terminal site more distal to CIRB (Singh *et al.*, 2002) as well as prolongation of delay of SOC activation via a common binding site for CaM and IP_3R, mostly likely CIRB (Vaca and Sampieri, 2002). As for other TRPC members, both spontaneous and agonist-induced activities of TRPC5 channel have been shown to be enhanced by Ca^{2+} entering through the channel itself (Okada *et al.*, 1998; Yamada *et al*., 2000), which are also potentiated directly by extracellular Ca^{2+} (and lanthanides; Jung *et al.*, 2003), as has been found in several native ROC channels (e.g. Inoue, 1991; Helliwell and Large, 1998; Aromolaran and Large, 1999). Furthermore, preliminary results have indicated that the magnitude of agonist-induced TRPC6 currents dramatically changes in response to extracellularly applied Ca^{2+} with complex time course (Inoue *et al.*, 2001). These findings strongly

suggest that Ca^{2+}-mediated regulation from both sides of the cell membrane may be a powerful and common means to modulate TRPC channel activities.

There is now growing body of evidence that TRPC6 is broadly distributed in extra-brain tissues, especially enriched in vascular smooth muscles, and may function as an integral subunit of native ROC channels activated via sympathetic nerve excitation, intravascular pressure increase and vasoactive peptides and growth hormones (Inoue *et al.*, 2001; Jung *et al*., 2002; Welsh *et al.*, 2002; Inoue *et al*., 2004). Despite this potential importance, little detailed information is yet available as to how Ca^{2+} modulates TRPC6 channel activities, although a recent Ca^{2+} fluorometric study has reported that a CaM-mediated mechanism is involved in positive modulation of this channel (Boulay, 2002). The present study was thus initiated to gain more insight for the complex actions of extra- and intracellular Ca^{2+} on TRPC6 channels in comparison with TRPC7, another member of the same subfamily which exhibits contrasting responses to Ca^{2+}, in terms of whole-cell and single channel recordings. As the results, we have found that TRPC6 and TRPC7 channels undergo effective but differential regulation by extra- and intracellular Ca^{2+} in CaM-dependent and -independent manners. Part of this study has been communicated to the 76th annual meeting of the Japanese Pharmacological Society (Shi *et al*., 2003).

Materials and Methods

Cell culture and Transfection

Human Embryonic Kidney293 (HEK293) cells were maintained in Dulbecco's modified Eagle's medium (DMEM) supplemented with 10% fetal bovine serum. For transfection, the cells were reseeded in a 35 mm culture dish and allowed to grow to 40-60% confluency, and then transfected with a mixture of 2μg plasmid vector (pCI-neo) incorporating TRPC DNAs (murine TRPC6, murine TRPC7 or their six chimeras; see below) and 0.4μg pCI-neo-πH3-CD8 (cDNA of the T-cell antigen CD8), with the aid of 20μl of the transfection reagent SuperFect^{TM} (Qiagen, Germany). In some experiments, 2μg of plasmid DNA for mutant calmodulin (mutCaM; see below) was co-transfected. About 24h after transfection, cells were reseeded onto coverslips precoated with 100μM poly-L-lysine. Electrophysiological measurements were performed within 48-72 h after transfection.

Construction of TRPC6/7 chimeras and mutant calmodulin (mutCaM)

The TRPC6/7 chimeras and the calmodulin mutant (mutCaM) were constructed by using PCR. In T667, the amino acid sequence 1-726 containing the N-terminus (1-402) and the hydrophobic core H1-H8 (403-726) of murine TRPC6 (Mori *et al.*, 1998) was linked to the C-terminal sequence 673-862 of murine TRPC7 (Okada *et al.*, 1999). In T776, the TRPC7 sequence 1-672 containing the N-terminus (1-348) and H1-H8 (349-672) was linked to the TRPC6 C-terminus 727-930. For the design of other chimeras, see the diagram in supplementary Fig.1. In mutCaM, aspartate residues 21, 57,

94, and 130 in 4 E-F hands were replaced with alanine to ablate Ca^{2+}-binding ability of calmodulin.

Electrophysiology

The details of three variants of patch clamp technique employed in this study (i.e. nystatin-perforated, conventional whole-cell, and single channel recordings) are essentially the same as described elsewhere (see supplementary information in Inoue *et al.*, 2001). Leak currents were estimated by constructing the current-voltage relationship in non-transfected cells. However, in successful recordings, the leak current estimated in this way was as small as 0.14 ± 0.05pA/pF at -60mV (n=15), and thus not corrected in the present study. For single channel recordings, pipette electrodes having a resistance of 5-10MΩ , 4-5 MΩ and 1.5-2MΩ (with pipette solution described below) were used in cell-attached (C/A), outside-out (O/O) and inside-out (I/O) configurations, respectively, while for whole-cell recordings, the pipette input resistance was 2.5-4 MΩ. Voltage generation and current signal acquisition were implemented through a high-impedance low-noise patch clamp amplifier (EPC9; HEKA Electronic, Germany). Sampled data were low-pass filtered at 1kHz (I/O, O/O) or 2kHz (C/A) and stored on a computer hard disc after digitization at 2-5kHz (I/O, O/O) or 20kHz (C/A). Long-term recordings (>30s; e.g. whole-cell currents in Fig.1) were performed in conjunction with an A/D, D/A converter Powerlab/400 (AD Instruments, South Wales, Australia; sampling rate: 100Hz) and data evaluation was made by the attached software ‘Chart v3.6’. Concentration-response relationships were fitted by a non-linear least square

routine, using two types of Hill equation. For single Hill fitting:

$$I=1.0/[1+(C/IC_{50})^{n}]$$

where I, C, IC_{50}, and n denote the normalized current amplitude (the ratio of currents after to before drug application), drug concentration, half maximal inhibitory concentration and cooperativity factor, respectively.

For double Hill fitting (Fig.2):

$$I=[1+ \Delta I/[1+(EC_{50}/C)^{n'}]/[1+(C/IC_{50})^{n}]$$

where I, C, IC_{50}, and n have the same meaning as described above, while ΔI, EC_{50} and n' denote the normalized current increase, half maximal effective concentration and cooperativity factor, respectively. It should however be mentioned that the fitting using this equation could provide only approximate values for EC_{50} and IC_{50}, since the results of double nonlinear fitting were prone to small changes in data points of a limited number.

Single channel analysis was made using the software 'Pulsefit' and/or a freely distributed web software 'Win/EDR v.2.3' (Dr. J. Dempster, University of Strathclyde, UK). To evaluate the unitary current amplitude, all-points or all-points-in-open-state amplitude histograms were constructed. To calculate the relative open probability (NPo), single channel currents were averaged for each 3-5s time interval and then converted to the NPo value according to the following equation:

$$I=i*N*Po$$

where I, i, N and Po denote the averaged single channel current, unitary amplitude, the

number of open channels and their open probability, respectively. The baseline for channel opening was normally determined by constructing all-point histograms, but when this was unfeasible due to baseline drifts, the records were divided into several segments, each of which was corrected for its linear trend by visual inspection. In the case of large I/O or O/O patch experiments where precise evaluation of unitary amplitude (i) was often difficult due to multiple channel openings, we adopted the averaged 'i' value determined by C/A recordings.

Solutions

Solutions with the following composition were used. Pipette solution for nystatin-perforated recording (in mM): 140CsCl, 2$MgCl_2$, 10HEPES, 10glucose (adjusted to pH 7.2 with Tris base). Internal solution for conventional whole-cell recording and O/O recording (in mM): 120CsOH, 120aspartate, 20CsCl, 2$MgCl_2$, 10BAPTA, 4$CaCl_2$, 10HEPES, 2ATP, 0.1GTP, 10glucose (adjusted to pH7.2 with Tris base; [Ca^{2+}]=ca. 80nM; '10BAPTA/4Ca-interenal solution'). In some experiments in which the effects of a broader range of [Ca^{2+}]$_i$ were investigated (e.g. Fig.5A and 6A), [Ca^{2+}] was adjusted by using 10mM BAPTA and appropriate concentrations of Ca^{2+} as performed in I/O recordings (see below). In Fig.8 and 9, in order to only weakly buffer [Ca^{2+}]$_i$, 10mMBAPTA was replaced by 0.1mM EGTA and 0.04mM Ca^{2+} added; adjusted to pH 7.2 with Tris base; '0.1EGTA-internal solution'). Ca^{2+} -free external solution (in mM): 140NaCl, 5KCl, 1.2$MgCl_2$, 1EGTA, 10HEPES, 10glucose (pH 7.4, adjusted with Tris base). For Ca^{2+}- , Sr^{2+}, or Ba^{2+}-containing external solutions, various

concentrations of $CaCl_2$, $SrCl_2$ or $BaCl_2$ were added to the Ca^{2+}-free solution with the omission of EGTA. Unless otherwise stated, pipette solution for C/A and I/O recordings contained (in mM): 140NaCl, 5 tetraethylammonium-Cl, 1.2$MgCl_2$, 0.1$CaCl_2$, 10HEPES, 10glucose, 0.1carbacol (CCh) (pH 7.4, adjusted with Tris base). 0.1mM Ca^{2+} was usually necessary to successfully obtain the 'giga' seal. For C/A recording, cells were bathed in high potassium solution with the following composition to null the transmembrane potential (in mM): 140KCl, 2EGTA, 2$MgCl_2$, 10HEPES (pH 7.2, adjusted with Tris base). Bathing solution for I/O recording (in mM): 120CsOH, 120aspartate, 20CsCl, 2$MgSO_4$, 2EGTA, 10HEPES, 2ATP, 0.1GTP (pH 7.2, adjusted with Tris base). To obtain the micromolar range [Ca^{2+}], a low affinity buffer HEDTA rather than EGTA was used. The amount of Ca^{2+} required to obtain the desired [Ca^{2+}] was calculated using Fabiato and Fabiato's program with enthalpic and ionic strength corrections (Brooks and Storey, 1992), as performed previously (Inoue and Ito, 2000).

In whole-cell, O/O and I/O single channel recordings, solutions were rapidly applied through a solenoid-driven fast solution change device 'Y-tube' (Inoue *et al.*, 2001).

Chemicals

Calmidazolium (chloride salt), OAG, 5'-adenylylimidodiphosphate (AMP-PNP), GTPγS, calmodulin, KN-62, okadaic acid, FK506, CaM-kinase II inhibitory peptide [CAMK-$IP_{(281-309)}$], myosin light chain kinase (MLCK) inhibitory peptide [MLCK-$IP_{(11-19)}$], and protein kinase C inhibitory peptide [PKC-$IP_{(19-36)}$] were purchased from Calbiochem (La Jolla, Canada), carbachol, HEPES, $SrCl_2$, $BaCl_2$ and

PDBu from Sigma (St. Louis, USA), ATP, GTP, BAPTA and EGTA from Dojindo (Kumamoto, Japan), and MLCK inhibitory peptide [$MLCK_{(11-19)}$ amide] from Alexis (Nottingham, UK). HEDTA was kindly provided by BASF Japan, Ltd.

Statistics

All data are expressed as mean ± s.e.m.. To evaluate statistical significance of the difference between a given set of data, paired and unpaired *t*-tests, and one way ANOVA with pooled variance *t*-test (Bonferroni's correction) were employed for single and multiple comparisons, respectively.

Results

Multiple effects of Ca^{2+} on heterologously expressed TRPC6 currents

Under quasi-physiological conditions with nystatin-perforated voltage-clamp (Horn and Marty, 1988; -60mV), human embryonic kidney 293 (HEK293) cells expressing murine TRPC6 differentially responded to muscarinic receptor stimulation (carbachol; CCh 100μM) at different levels of external Ca^{2+} (Ca^{2+}_o) (Fig.1A). The time courses of activation and inactivation of CCh-induced current (I_{TRPC6}) evaluated in the same cell were clearly faster in the presence of 1mM Ca^{2+}_o as compared with its absence. Paired data from 12 cells indicate that three parameters representing the rates of activation and inactivation, t_{10}, t_{10-90} and t_{90-50}, are significantly shorter in the presence of Ca^{2+}_o (Fig.1B). The extent of maximum activation (i.e. peak amplitude) was also greater with 1mM Ca^{2+} in the bath (25.7± 2.8 vs. 37.8± 4.9pA/pF at -60mV, n=12; $P<0.05$ with paired t-test). These results show that the presence of Ca^{2+}_o enhances the extent of activation and accelerates the activation and inactivation processes of I_{TRPC6}. Similar enhancement and acceleration of activation (or potentiation) and of inactivation were observed, when Ca^{2+}_o was added after I_{TRPC6} had already reached the peak activation (Fig.1C). In this case, however, in addition to slower potentiating and inactivating phases (#), an immediate increase in I_{TRPC6} amplitude (*-*), which was not discernible in the continued presence of Ca^{2+}_o (Fig.1A), was also visualized.

The potentiating and inactivating effects of Ca^{2+}_o on I_{TRPC6} were still observed, when conventional whole-cell recording with weak Ca^{2+} buffering capacity (0.1EGTA-internal solution) was used (data not shown). However, inclusion of 10mM

BAPTA in the pipette (10BAPTA/4Ca-internal solution; calculated $[Ca^{2+}]_i$=80nM; conventional whole-cell clamp mode) selectively abolished the slow potentiating and inactivating effects of Ca^{2+}_o on I_{TRPC6} without affecting the fast potentiating actions (Fig.1D and E), suggesting that the slow effects of Ca^{2+}_o are mediated by elevation in $[Ca^{2+}]_i$. Under these conditions, the effects of Ca^{2+}_o on I_{TRPC6} occurred as a biphasic function of $[Ca^{2+}]_o$ characterized by potentiation in submilli- to milli-molar range (<1-3mM; apparent EC_{50}; ~0.4mM) and inhibition in a higher concentration range (>1-3mM; apparent IC_{50}; ~4mM) (Fig.2A and C). These Ca^{2+}_o effects most likely result from the actions on TRPC6 channel per se, since comparable $[Ca^{2+}]_o$-dependence was observed when I_{TRPC6} was more directly activated by GTPγS or OAG, by bypassing the receptor, G-protein or phospholipase C (PLC) (Fig.2B and C). Similar biphasic (but less pronounced) effects on I_{TRPC6} were also observed for Sr^{2+}, but were virtually absent for another Ca^{2+}-mimetic Ba^{2+} (Fig.2D-F).

The rapidity and resistance to vigorous $[Ca^{2+}]_i$ buffering of fast potentiation and inhibition by Ca^{2+} and Sr^{2+} suggest that their site(s) of actions may reside at the extracellular side of TRPC6 channel. In strong support of this idea, the extent of potentiation and inhibition did not change by clamping $[Ca^{2+}]_i$ to a more elevated level (2μM ; filled circles in Fig.2C), and quantitatively comparable effects of Ca^{2+}_o could still be obtained on single TRPC6 channel activities recorded in cell-free, outside-out (O/O) patch configuration (Fig.3A and B).

The current-voltage (I-V) relationships for macroscopic I_{TRPC6} show that the fast inhibition by high millimolar Ca^{2+}_o occurs via a voltage-dependent mechanism; the

extent of the inhibition was significantly decreased at strongly depolarized membrane potentials (dotted vs. thin solid curves in Fig.3C; % inhibition by 10mM Ca^{2+}_o relative to 0mM: 75±5% at -100mV, 42±6% at 100mV, n=7; $P<0.05$). This voltage-dependence can be accounted for at least in part by voltage-dependent reductions of the unitary conductance and degree of activation (NPo) of single TRPC6 channel, since both reductions were relieved at strongly depolarized potentials (Fig.3D; open triangles in Fig.3E; Fig.3F). In contrast, the fast potentiation of I_{TRPC6} at sub- to low millimolar Ca^{2+}_o exhibited little sign of voltage-dependence, as evidenced by almost symmetrically increased I-V relationship (dotted vs. bold solid curves in Fig.3C) and unaltered unitary amplitude or NPo values at different potentials (filled circles in Fig.3E; Fig.3F). These results suggest that the mechanism underlying the potentiation may be different from that for the inhibition, but in the present study, we could not unequivocally figure out what changes in single channel properties contribute to the former.

Ca^{2+}_o inhibits TRPC7 channels.

TRPC7 is a closest homologue of TRPC6 and has been shown to exhibit much higher spontaneous activities than TRPC6 and undergo inhibitory actions of Ca^{2+}_o (Okada *et al.*, 1999). As demonstrated in Fig.4, over a broad range of $[Ca^{2+}]_o$, Ca^{2+}_o merely caused a concentration-dependent inhibition of currents due to TRPC7 expression (spontaneous plus CCh-induced currents; I_{TRPC7}), irrespective of the species of activators used (i.e. CCh, GTPγS, OAG; Fig.4A and B). Part of this inhibition was however eliminated by increasing the buffering capacity for $[Ca^{2+}]_i$ (Fig.4A vs. B; open vs. filled circles: * in

Fig.4B), suggesting the involvement of elevated $[Ca^{2+}]_i$ in $Ca^{2+}{}_o$-induced inhibition.

The fast inhibition of I_{TRPC7} remaining after strongly $[Ca^{2+}]_i$-buffering occurred in about a 10-fold lower concentration range of $Ca^{2+}{}_o$ (apparent IC_{50}: 0.44mM) as compared with I_{TRPC6}, but showed a very similar voltage-dependency to I_{TRPC6}, being characterized by more prominent inhibition of macroscopic I-V relationship and reductions of unitary conductance and NPo at negative potentials (Fig.4C-F). Furthermore, exchanging the transmembrane (TM) region of TRPC7 with that of TRPC6 converted the fast inhibition caused by 1mM Ca^{2+} to potentiation (supplementary Fig.1). Taken together, these results are consistent with the idea that the site(s) of fast $Ca^{2+}{}_o$ actions are located on the extracellular side of TM region, of which only an inhibitory site may commonly exist in TRPC6 and 7 channels.

Mechanisms involved in intracellular Ca^{2+}'s actions on TRPC6 and TRPC7 channels

The abolition of slow potentiating and inactivating effects of $Ca^{2+}{}_o$ on I_{TRPC6} by vigorous $[Ca^{2+}]_i$ buffering implies that the level of $[Ca^{2+}]_i$ may both positively and negatively regulate TRPC6 channel activities. Consistent with this speculation, when cells were intracellularly perfused with various values of $[Ca^{2+}]_i$, the density of CCh-induced I_{TRPC6} showed a biphasic dependence on $[Ca^{2+}]_i$ consisting of incremental (<~200nM) and decremental (>~200nM) phases (Fig.5A). A similar $[Ca^{2+}]_i$ dependence was also observed for I_{TRPC7}, but in this case, the range for positive regulation is shifted to much lower concentrations as compared with I_{TRPC6} (Fig.6A). The $[Ca^{2+}]_i$ dependence of TRPC6 and TRPC7 channels did not change appreciably, even when they were

activated by OAG (data not shown). It seems thus likely that the site(s) of the actions of intracellular Ca^{2+} (Ca^{2+}_i) are also located on the channel proteins themselves.

Calmodulin (CaM) is a ubiquitous intracellular calcium-binding protein involved in Ca^{2+}-mediated regulation of many ionic channels (Levitan, 1999; Saimi and Kung, 2001). In addition to direct binding to channel proteins, the Ca^{2+}-bound CaM (Ca^{2+}/CaM) activates several physiologically important kinases and phosphatases including CaM-kinase II, myosin light chain kinase (MLCK) and calcineurin, thereby altering the phosphorylated state of channel proteins to modulate their functions (Braun and Schulman, 1995a; Kamm and Stull, 2001; Rusnak and Mertz, 2000). To assess the potential importance of these mechanisms in Ca^{2+}_i-mediated regulation of TRPC6 and TRPC7 described above, we next tested how inhibitors for CaM and Ca^{2+}/CaM-dependent enzymes affect these channel functions.

Pretreatment of TRPC6-expressing cells with calmidazolium (CMZ; 3μM), a potent CaM antagonist (IC_{50}:~10nM), or coexpression of a Ca^{2+}-insensitive mutant of CaM (mutCaM), strongly attenuated the activation of I_{TRPC6} by CCh, GTPγS or OAG. (Fig.5B and C). Such a marked attenuation also occurred by decreasing $[Ca^{2+}]_i$ to an extremely low level (<10nM; Fig.5A), by pretreatment with an organic CaM kinase II inhibitor KN-62 (2μM), or with intracellular perfusion of CaM-kinase II inhibitory peptide [CAMK-$IP_{(281-309)}$; Fig.5D]. Furthermore, substitution of ATP with its non-hydrolyzable analogue AMP-PNP in the patch pipette solution dramatically reduced the I_{TRPC6} density (Fig.5D). These results collectively suggest that phosphorylation by CaM kinase II is a prerequisite for activation of TRPC6 channel. In contrast, inhibitory peptides for MLCK

[MLCK-IP$_{(11-19)}$, MLCK-IP$_{(480-501)}$], a nonspecific protein phosphatase inhibitor okadaic acid (10μM) or a potent calcineurin inhibitor FK506 (1μM) did not significantly affect the I_{TRPC6} density (Fig.5D).

In sharp contrast with the critical importance of CaM kinase II for TRPC6 activation, activation of I_{TRPC7} by CCh was not impaired by pretreatment with CMZ (3μM) or co-expression of mutCaM, but rather enhanced (Fig.6B and C; however, spontaneous I_{TRPC7} did not exhibit a significant increase; not shown). Inhibitors for CaM kinase II, MLCK and calcineurin were also all ineffective to affect I_{TRPC7} (Fig.6E). These results exclude the requirement of Ca^{2+}/CaM and phosphorylation for TRPC7 channel activation. However, the extent of Ca^{2+}_o (1mM)-induced inhibition of I_{TRPC7} was significantly reduced by pretreatment with CMZ or coexpression of mutCaM (Fig.6D), being comparable to that observed for strongly $[Ca^{2+}]_i$-buffering conditions (Fig.4B). This observation suggests the presence of some inhibitory actions of Ca^{2+}/CaM on TRPC7 channels. To elucidate these actions more directly, we next employed the inside-out (I/O) configuration of single channel recording.

Ca^{2+}/CaM actions on TRPC6 and 7 channels.

Single TRPC6 or TRPC7 channels recorded in I/O mode with patch pipettes in ordinary size (5-10MΩ) showed a rapid rundown, which presumably reflects a gradual loss of intracellular constituents maintaining the channel activities (i.e. washout phenomenon). To circumvent this problem, we needed to use patch pipettes having a very low input resistance (1.5 - 2MΩ), by which, in more than 30% of patch membranes tested, the

decline of channel activities could be minimized over a period of 5-10 minutes.

Fig.7 demonstrates typical examples of CCh (100μM)-activated TRPC6 and TRPC7 channel activities at various $[Ca^{2+}]_i$ levels (I/O mode). The activity of TRPC7 channel was decreased by elevation of $[Ca^{2+}]_i$ in the nanomolar range (<10-110nM) and completely suppressed by further increase in $[Ca^{2+}]_i$ (Fig.7A and open circles in E). TRPC6 channels was also subject to inhibition by $Ca^{2+}{}_i$ but required more than 10-fold higher $[Ca^{2+}]_i$ (1.45μM) than TRPC7 to be significantly inhibited (Fig.7B vs. F). $Ca^{2+}{}_i$-mediated inhibition of TRPC7 channel activities were strongly attenuated by pretreatment with CMZ (3μM) or coexpression of mutCaM. As demonstrated in Fig.7C, application of CMZ in C/A configuration gradually enhanced TRPC7 channel activities, which showed, after excision of patch membrane (i.e. I/O mode), a much decreased sensitivity to $Ca^{2+}{}_i$; the effective range of $[Ca^{2+}]_i$ to inhibit TRPC7 channels was shifted from nano- to micromolar concentrations (filled circles in Fig.7E). A similar shift was also observed with coexpression of mutCaM (Fig.7E). These results strongly suggest that TRPC7 channel activities are negatively regulated by Ca^{2+}/CaM.

The effects of CMZ and mutCaM on single TRPC6 channels were entirely different from those on TRPC7 channels. Consistent with their effects observed for macroscopic I_{TRPC6}, application of CMZ greatly diminished the CCh-induced TRPC6 channel activities in C/A mode, and subsequent exposure of excised membrane to various $[Ca^{2+}]_i$ levels (I/O mode) could not restore the channel activities (Fig.7D and F). Coexpression of mutCaM produced essentially the same results (Fig.7F). These results confirm that Ca^{2+}/CaM-mediated process is obligatory for TRPC6 channel activation. However, we

cannot exclude the possibility that inhibition by Ca^{2+}/CaM observed at micromolar $[Ca^{2+}]_i$, which were not experimentally seen after abolition of activation process, may also exert some modulatory role on TRPC6 channels.

The mechanism for the negative regulation of TRPC7 channels by Ca^{2+}/CaM seems compatible with a recently proposed hypothesis of competitive regulation by CaM and IP_3 of TRPC3 for its common binding domain (e.g. CIRB; see Introduction). Addition of IP_3 (10μM) increased single TRPC7 activities, and this was significantly counteracted by elevated $[Ca^{2+}]_i$ or exogenously applied CaM (1μM) (Fig.8A and B). Macroscopic I_{TRPC7} evoked by CCh or OAG was also greatly enhanced by intracellular perfusion of IP_3 (Fig.8D; there was however no dramatic increase in spontaneous I_{TRPC7}; 5.5±1.4 vs. 7.4±1.3pA/pF without and with 10μM IP_3, respectively; n=7). In contrast, IP_3 exerted little effects on TRPC6 at either whole-cell or single channel levels (Fig.8B and D). Instead, as reported recently (Estacion *et al*, 2004), marked enhancement of OAG-induced I_{TRPC6} occurred by pretreatment with a subthreshold activating concentration of CCh (0.5μM; Fig.8C and D). At least under our experimental conditions, the major part of this enhancement seems ascribable to synergistic effects of $Ca^{2+}{}_i$, as it was observed only with weak $[Ca^{2+}]_i$-buffering; OAG (100μM)-induced I_{TRPC6} recorded with 10BAPTA/4Ca-internal solution was not significantly affected by pretreatment with 0.5μM CCh [at -60mV; 27.0 ± 6.7pA/pF (n=5) vs. 26.3 ± 4.8pA/pF (n=6) for control and 0.5μM CCh pretreatment, respectively].

Differential regulation by Ca^{2+}/CaM and IP_3 observed between TRPC7 and 6 channels likely reflects their C-terminal differences. Their chimeras with exchanged

C-termini T667 and T776 showed essentially the same dependence on Ca^{2+}/CaM and IP_3 as TRPC7 and TRPC6, respectively (supplementary Fig.2).

Involvement of PKC in TRPC6 inactivation.

According to previous studies (Trebak *et al*., 2003; Estacion *et al*, 2004), protein kinase C (PKC) negatively regulates some TRPC members including TRPC6. This raises a possibility that activation of PKC may be involved in the rapid inactivation process of I_{TRPC6} in the presence of Ca^{2+}_o (Fig.1A and B) and its decreased current density at micromolar $[Ca^{2+}]_i$ (Fig.5). Consistent with this expectation, inclusion of a PKC inhibitor, calphostin C (500nM) or a PKC inhibitory peptide [PKC-$IP_{(19-36)}$: 5μM] in the patch pipette significantly decelerated the time course of inactivation (or decreased τ_{10-90} value; Fig.9A and B) and enhanced the I_{TRPC6} density at micromolar $[Ca^{2+}]_i$ (Fig.9C). Conversely, activation of PKC by a phorbol ester, PDBu (1μM; pretreated 10min), caused almost complete suppression of I_{TRPC6} (Fig.9C). Similar enhancement of current density by PKC inhibitors and inhibition by PDBu were also observed for I_{TRPC7} (Fig.9C).

Discussion

TRPC6 and 7 share more than 70% identity in the overall amino acid sequence (N-terminus: 80%; transmembrane region: 77%; C-terminus: 73%) and both code for Ca^{2+}-permeable cation channels activated by diacylglycerol (Hofmann *et al.*, 1999; Okada *et al.*, 1999). Despite these molecular and functional similarities, the results of the present study have provided the evidence that heterologously expressed TRPC6 and 7 channels undergo contrasting regulations by Ca^{2+} from both extracellular and intracellular sides, via CaM-dependent and -independent mechanisms.

Whole-cell (with 10mM BAPTA) and single channel data (Fig. 4) together suggest that the most part of fast voltage-dependent inhibitory actions by Ca^{2+}_o on I_{TRPC7} is ascribable to its interaction with an 'extracellular' site(s) which can sense the transmembrane potential. A similar inhibitory site having a weaker efficacy is likely present in TRPC6 channels (Fig.2 and 3). In contrast, the fast potentiating effect of Ca^{2+}_o is unique to TRPC6 and did not show voltage-dependence and were not associated with changes in unitary conductance (compare 0.1 and 1mM in Fig.3E), but also likely occur through the extracellular actions of Ca^{2+}, as unequivocally demonstrated by the O/O recording (Fig.2A and B). The finding that the type of TM region critically determines the pattern of response to Ca^{2+}_o (i.e. 'inhibitory' or 'facilitatory'; supplementary Fig.1) further reinforces this speculation. These extracellular Ca^{2+} effects may most simplistically be accounted for by the permeation blockade and/or stabilization of gating in 'non-conductive' states by Ca^{2+}_o, which are often found in

many cation-selective channels (e.g. Hille, 2001).

Complex extracellular actions of Ca^{2+} and of its mimetics lanthanides (La^{3+} and Gd^{3+}), which are strongly reminiscent of Ca^{2+}_o actions on TRPC6 and 7, have recently been reported for heterologously expressed mouse TRPC5 channel (Jung *et al.*, 2003). In this channel, the effect of lanthanides is biphasic with concentration-dependent potentiation in the low micromolar range and inhibition in a higher concentration range, whereas that of Ca^{2+} is merely facilitatory only at high millimolar concentrations. Site-directed mutagenesis has revealed that three glutamate residues adjacent to the putative pore-forming loop (Glu^{543}, Glu^{595}, Glu^{598}) are crucial for the observed La^{3+}- as well as Ca^{2+}-induced potentiation (Jung *et al.*, 2003). However, alignments of TM5-TM6 linker region of TRPC5, 6 and 7 (supplementary Fig.3) indicate little similarity present for these glutamates between the three TRPC channels (see also Jung *et al.*, 2003). Except for Glu^{598}, negatively charged residues corresponding to Glu^{543} or Glu^{595} are absent in TRPC6 and 7, which instead possess four additional glutamates or aspartate in more central part. Furthermore, the overall amino acid sequence of TRPC6 and 7 in this linker region, especially the number and position of negatively charged residues, is highly homologous (supplementary Fig.3), thus suggesting that these residues might not suffice to elucidate the differential effects of Ca^{2+}_o on TRPC6 and 7 channels.

The observed $[Ca^{2+}]_o$-sensitivity of recombinant TRPC6 channel is substantially different from that reported for a number of native ROC channels in which this protein is likely involved (Inoue *et al.*, 2001; Jung *et al.*, 2002). For instance, the

α1-adrenonceptor-activated cationic channel (α1-AD-NSCC) in portal vein smooth muscle displays much higher sensitivity to Ca^{2+}_o potentiation (EC_{50}=3μM) showing a rapid declining feature (Helliwell and Large, 1998), and is also potentiated by submillimolar concentrations of Ba^{2+} and Sr^{2+} (Aromolaran and Large, 1999). However, in the present study, Ba^{2+} was found ineffective to cause either potentiation or inhibition of expressed TRPC6 channels, and their potentiation by Ca^{2+} and Sr^{2+} was rather long-lasting (Fig.1D and Fig.2D). A more strikingly different $[Ca^{2+}]_o$ sensitivity is found for TRPC6-like currents in A7r5 cells, where millimolar Ca^{2+}_o exerts only inhibitory actions, although reduction of this current by changing $[Ca^{2+}]_o$ from 200μM to nominally zero suggests a stimulatory role of Ca^{2+}_o (Ba^{2+} and Sr^{2+} are however ineffective; Jung *et al.*, 2002). A possible molecular background for such discrepancies is that these native TRPC6-like channels may be heteromultimerically assembled with other endogenously expressed TRP isoforms, thereby acquiring diverse divalent cation sensitivities. In support of this possibility, TRPC6 has been shown to co-immunoprecipitate with TRPC3 and 7 in adult tissues (Hofmann *et al.*, 2002; Goel *et al.*, 2002) and in embryonic brain interact with other TRPC isoforms in complex combinations (Strübing *et al.*, 2003), and the presence of some of these isoforms has been confirmed by RT-PCR technique in portal vein myocytes and A7r5 cells (Inoue *et al.*, 2001; Jung *et al.*, 2002). However, it should be noted that the expression system used in this study (HEK293 cells) has been reported to endogenously express several TRPC isoforms including TRPC1, 3, 4 and 6 (Garcia and Schilling, 1997). Considering this fact, we cannot completely exclude the possibility that overexpressed TRPC6 or 7

channels could also be affected by these endogenously TRPC proteins thus bearing somewhat altered properties as compared with genuine homomeric channels.

Single channel data in large I/O membranes have indicated that, once receptor-activated, TRPC7 channels are concentration-dependently inhibited by Ca^{2+}_i of nanomolar range. These effects are likely mediated via CaM-dependent actions on its C-terminus, as indicated by mutCaM coexpression and TRPC6/7 chimera experiments. Previous biochemical studies have shown that all TRPC members possess a common binding region for CaM and IP_3 receptor (IP_3R) on the C-terminus (CIRB domain), to which CaM binds in a strictly Ca^{2+}-dependent manner (Tang *et al.*, 2001). It has been hypothesized that under resting conditions, CaM bound to this region tonically inhibits TRPC3 channels, and its displacement by activated IP_3R (by receptor stimulation) or its inactivation by the CaM antagonist CMZ leads to channel activation (Zhang *et al.*, 2001). Overall, this picture seems to apply to TRPC7; pretreatment with CMZ or coexpression of mutCaM enhanced CCh-activated TRPC7 channel activities at both single channel (C/A mode; Fig.7) and whole-cell (Fig.6) levels; in I/O recording, inhibitory effects of Ca^{2+}_i, on TRPC7 channel, which were strongly attenuated by CMZ or mutCaM (Fig.7), were antagonized and enhanced by IP_3 and CaM, respectively (Fig.8). However, the observed $[Ca^{2+}]_i$ range for CaM-dependent TRPC7 channel inhibition (apparent IC_{50}=~100nM; Fig.7) is far lower when compared to the Ca^{2+}-dependence of CaM binding domain (i.e. CIRB) evaluated in vitro (Tang *et al.*, 2001). The effect of Ca^{2+}_i still persisted even after exposure to a very low $[Ca^{2+}]_i$ level

(<10nM) which was expected to unbound CaM (Fig.7A). Coexpression of mutCaM enhanced the magnitude of I_{TRPC7}, but did not appreciably induce a current by itself unless the receptor is stimulated (e.g. Fig.6B). All these findings are not simply compatible with the antagonism between CaM and IP_3R for channel activation (Zhang *et al.*, 2001). The most straightforward interpretation of the above results is that CaM is constitutively bound to TRPC7 channel C-terminus and negatively regulates the channel activity in a Ca^{2+}-dependent fashion regardless of receptor activation process. Thus, the role of CaM would not be obligatory for TRPC7 channel activation but rather modulatory as a negative feedback operating during receptor stimulation. However, despite that the observed $[Ca^{2+}]_i$ range for negative regulation of single TRPC7 channels (Fig.7E) roughly matches that for I_{TRPC7} (Fig.6A), at an extremely low $[Ca^{2+}]_i$ (<10nM), receptor-activation of I_{TRPC7} was severely impaired. This is unexpected from single channel recordings, and unlikely involves the actions of CaM, IP_3R or phosphorylation e.g. by CAMKII (see above). It seems thus likely that an additional, as-yet-unidentified, Ca^{2+}-dependent mechanism participates in the activation process of TRPC7 channels.

Despite the presence of almost identical CaM binding domain (CIRB; Tang *et al.*, 2001), the inhibitory effect of $Ca^{2+}{}_i$ on single TRPC6 channels is much weaker than TRPC7 (occurred only at micromolar $[Ca^{2+}]_i$), and intracellular application of IP_3 failed to activate or enhance the channel activities at whole-cell and single channel levels (Fig.8). This excludes the involvement of competitive regulation by Ca^{2+}/CaM and IP_3R in TRPC6 channel activation process. Instead, we have found that activation of

macroscopic TRPC6 current is positively regulated by nanomolar Ca^{2+}_i and highly susceptible to procedures that eliminate intracellular ATP and CaM or directly inhibit CAMKII, regardless of the activator (i.e. CCh or OAG) (Fig.5, 7). These results are consistent with the idea that phosphorylation by CaMKII is an obligatory step for TRPC6 channel activation and occurs independently of the process to generate DAG. Similar CaMKII phosphorylation-mediated activation has also been reported for epithelial Ca^{2+}-activated nonselective cation channels, the properties of which are strongly reminiscent of some TRP members (Braun and Schulman, 1995b).

Somewhat puzzlingly, however, activation of the native counterpart of TRPC6, α1-AD-NSCC in vascular smooth muscle, has been reported to be mediated by MLCK rather than CAMKII (Aromolaran *et al.*, 2000). In this native channel, MLCK-specific peptides, one of which [$MLCK_{(11-19)}$ amide] was found ineffective for expressed TRPC6 channel in this study, strongly prevented the activation of α1-AD-NSCC. One plausible explanation for this discrepancy is that rather muscle-specific distribution of MLCK may allow its preferential interaction with TRPC6 channel in muscle tissues (Kamm and Stull, 2001) whereas in other tissues, more ubiquitous CaMKII may play a similar role. However, it should be pointed out that while CaMKII can target a multitude of substrates including ion channels (Braun and Schulman, 1995a), the only known physiological target of MLCK is myosin, which is implicated in the regulation of muscle contraction and cytoskeletal activities but not directly in channel activation (Kamm and Stull, 2001). These discrepancies, together with the fact that synergism between IP_3 and OAG observed for α1-AD-NSCC activation (Albert and Large, 2003)

is deficient in expressed TRPC6 channels (Fig.8; Estacion *et al*., 2004), again suggest that essential differences may be present in subunit compositions or accessory regulatory mechanisms between these two channels. Obviously, more studies will be needed to elucidate the exact mechanism underlying phosphorylation-mediated activation of TRPC6 channel.

In summary, the activity of TRPC6 channel is likely regulated by Ca^{2+} in a multifold fashion. In physiological ionic milieu, in addition to direct tonic enhancement by Ca^{2+}_o, Ca^{2+}_i-dependent mechanisms seem to dynamically regulate TRPC6 channels during PLC-linked receptor stimulation. In the early phase, Ca^{2+} released from internal store via activated IP_3R and Ca^{2+} influx through activated TRPC6 channels by DAG generation elevate $[Ca^{2+}]_i$ thereby facilitating the channel activation process via CaMKII-mediated phosphorylation (Fig.5). When the elevation of $[Ca^{2+}]_i$ is sustained, however, this turns to inactivation via PKC activation (Fig.8). Such sequential activation of kinases can be seen as accelerated activation and inactivation processes by Ca^{2+}_o (Fig.1A and C). In contrast, Ca^{2+} regulates TRPC7 channels almost negatively via direct extracellular, and Ca^{2+}/CaM- (but phosphorylation-independent) and PKC-dependent mechanisms (Fig.4, 7 and 9). In this channel, generation of IP_3 seems to synergistically enhance the channel activity with its primary activator DAG (Fig.9).

Multifold regulation by Ca^{2+} reminiscent of TRPC6 has been reported for some native ROC channels. For instance, muscarinic cation channels in gastrointestinal smooth muscle has been shown to be strongly potentiated by $[Ca^{2+}]_i$ elevation (Inoue and Isenberg, 1990; Pacaud and Bolton, 1991), part of which may involve a

Ca^{2+}/CaM-MLCK dependent pathway (Kim *et al.*, 1995; Kim *et al.*, 1997). This mechanism seems to operate as an effective positive feedback synchronized with action potentials and IP_3-mediated intracellular Ca^{2+} release, contributing to enhanced excitatory actions of visceral cholinergic nerves on gut motility (Kuriyama *et al.*, 1998). In contrast, prolonged $[Ca^{2+}]_i$ elevation inactivates these channels and terminates the muscarinic response rapidly (Kim *et al*., 1998; Zholos *et al.*, 2003). A similar situation may hold for the α1-AD-NSCC in portal vein smooth muscle, in which molecular contribution of TRPC6 has been more unequivocally demonstrated (Inoue *et al.*, 2001; Large, 2002). In this respect, the results of this study would provide an important molecular basis for elucidating such multifold effects of Ca^{2+} in native tissues.

Acknowledgements

We thank Miss Yoko Takashiro for expert technical assistance. This study is supported in part by a grant-in-aid from the Ministry of Education, Culture and Science to R.I. J.S. is a fellow of the Tokyo Biochemical Research Foundation.

References

Albert AP, Large WA (2003). Synergism between inositol phosphates and diacylglycerol on native TRPC6-like channels in rabbit portal vein myocytes. *J Physiol* **552**, 789-795

Aromolaran AS, Albert AP, Large WA. (2000). Evidence for myosin light chain kinase mediating noradrenaline-evoked cation current in rabbit portal vein myocytes. *J Physiol* **524**, 853-863

Aromolaran AS & Large WA (1999). Comparison of the effects of divalent cations on the noradrenaline-evoked cation current in rabbit portal vein smooth muscle cells. *J Physiol* **520**, 771-782

Boulay G, Brown DM, Qin N, Jiang M, Dietrich A, Zhu MX, Chen Z, Birnbaumer M, Mikoshiba K & Birnbaumer L (1999). Modulation of Ca^{2+} entry by polypeptides of the inositol 1,4,5-trisphosphate receptor (IP3R) that bind transient receptor potential (TRP): evidence for roles of TRP and IP3R in store depletion-activated Ca^{2+} entry. *Proc Natl Acad Sci U S A* **96**, 14955-14960

Boulay G. (2002) Ca^{2+}-calmodulin regulates receptor-operated Ca^{2+} entry activity of TRPC6 in HEK-293 cells. *Cell Calcium* **32**, 201-207

Braun AP, Schulman H (1995a). The multifunctional calcium/calmodulin-dependent protein kinase: from form to function. *Annu Rev Physiol* **57**, 417-45

Braun AP, Schulman H (1995b). A non-selective cation current activated via the multifunctional Ca^{2+}-calmodulin-dependent protein kinase in human epithelial cells. *J Physiol* **488**, 37-55

Brooks SP & Storey KB (1992). Bound and determined: a computer program for making buffers of defined ion concentrations. *Anal Biochem* **14**,119-126

Clapham DE, Runnels LW & Strübing C (2001) The TRP ion channel family. *Nat Rev Neurosci* **2**, 387-396

Estacion M, Li S, Sinkins WG, Gosling M, Bahra P, Poll C, Westwick J, Schilling WP. (2004). Activation of human TRPC6 channels by receptor stimulation. *J Biol Chem* **279**, 22047-22056

Goel M, Sinkins WG & Schilling WP (2002). Selective association of TRPC channel subunits in rat brain synaptosomes. *J Biol Chem* **277**, 48303-48310

Garcia RL, Schilling WP. (1997). Differential expression of mammalian TRP homologues across tissues and cell lines. *Biochem Biophys Res Commun* **239**, 279-83.

Hardie RC (1995). Photolysis of caged Ca^{2+} facilitates and inactivates but does not directly excite light-sensitive channels in Drosophila photoreceptors. *J Neurosci* **15**, 889-902

Helliwell RM & Large WA (1998). Facilitatory effect of Ca^{2+} on the noradrenaline-evoked cation current in rabbit portal vein smooth muscle cells. *J Physiol* **512**, 731-741

Hille B (2001). *In*: Ion channels of excitable membranes. 3rd Edition, Sunauer Associates, Inc., Sunderland/Massachusetsetts

Hoffmann T, Obukhov AG., Schaefer M, Harteneck C, Gudermann T & Schultz G. (1999). Direct activation of human TRPC6 and TRPC3 channels by diacylglycerol.

Nature **397**, 259-263

Hofmann T, Schaefer M, Schultz G & Gudermann T (2002). Subunit composition of mammalian transient receptor potential channels in living cells. *Proc Natl Acad Sci U S A* **99**, 7461-7466

Horn, R., Marty, A. (1988). Muscarinic activation of ionic currents measured by a new whole-cell recording method. *J Gen Physiol* **92**, 145-159

Inoue R (1991). Effect of external Cd^{2+} and other divalent cations on carbachol-activated non-selective cation channels in guinea-pig ileum. *J Physiol* **442**, 447-63

Inoue R & Isenberg G. (1990). Intracellular calcium ions modulate acetylcholine-induced inward current in guinea-pig ileum. *J Physiol* **424**, 73-92

Inoue R, Morita H, Ito Y (2004). Newly emerging Ca^{2+} entry channel molecules that regulate the vascular tone. *Expert Opin Ther Targets* **8**, 321-334

Inoue R, Okada T, Onoue H, Hara Y, Shimizu S, Naitoh S, Ito Y & Mori Y (2001). The transient receptor potential protein homologue TRP6 is the essential component of vascular α_1–adrenocepotor-activated Ca^{2+}-permeable cation channel. *Circ Res* **88**, 325-332

Inoue R & Ito Y (2000). Intracellular ATP slows time-dependent decline of muscarinic cation current in guinea pig ileal smooth muscle. *Am J Physiol Cell Physiol* **279**, C1307-C1318

Jung S, Strotmann R, Schultz G & Plant TD (2002). TRPC6 is a candidate channel involved in receptor-stimulated cation currents in A7r5 smooth muscle cells.

Am J Physiol Cell Physiol **282**, C347-C359

Jung S, Mühle A, Schaefer M, Strotmann R, Schultz G & Plant T D (2003). Lanthanides potentiate TRPC5 currents by an action at extracellular sites close to the pore mouth. *J Biol Chem* **278**, 3562-3571

Kamm KE, Stull JT. (2001). Dedicated myosin light chain kinases with diverse cellular functions. *J Biol Chem* **276**, 4527-4530

Kamouchi M, Philipp S, Flockerzi V, Wissenbach U, Mamin A, Raeymaekers L, Eggermont J, Droogmans G & Nilius B (1999). Properties of heterologously expressed hTRP3 channels in bovine pulmonary artery endothelial cells. *J Physiol* **518**, 345-358.

Kim SJ, Ahn SC, So I & Kim KW (1995). Role of calmodulin in the activation of carbachol-activated cationic current in guinea-pig gastric antral myocytes. *Pflugers Arch* **430**, 757-762.

Kim YC, Kim SJ, Kang TM, Suh SH, So I & Kim KW (1997). Effects of myosin light chain kinase inhibitors on carbachol-activated nonselective cationic current in guinea-pig gastric myocytes. *Pflugers Arch* **434**, 346-353.

Kim YC, Kim SJ, Sim JH, Jun JY, Kang TM, Suh SH, So I & Kim KW (1998). Protein kinase C mediates the desensitization of CCh-activated nonselective cationic current in guinea-pig gastric myocytes. *Pflugers Arch* **436**, 1-8.

Kiselyov K, Xu X, Mozhayeva G, Kuo T, Pessah I, Mignery G, Zhu X, Birnbaumer L & Muallem S (1998). Functional interaction between $InsP_3$ receptors and store-operated Htrp3 channels. *Nature* **396**, 478-482

Kuriyama H, Kitamura K, Itoh T & Inoue R (1998). Physiological features of visceral smooth muscle cells, with special reference to receptors and ion channels. *Physiol Rev* **78**, 811-920

Large WA (2002). Receptor-operated Ca^{2+}-permeable nonselective cation channels in vascular smooth muscle: a physiologic perspective. *J Cardiovasc Electrophysiol* **13**, 493-501

Levitan IB (1999). It is calmodulin after all! Mediator of the calcium modulation of multiple ion channels. *Neuron* **22**, 645-648

Minke B & Cook B (2002). TRP channel proteins and signal transduction. *Physiol Rev* **82**, 429-472

Montell C (2001). Physiology, phylogeny, and functions of the TRP superfamily of cation channels. *Sci STKE*, www.stke.org/cgi/content/full/OC_sigtrans;2001/90/re1, pp. 1-17

Mori Y, Takada N, Okada T, Wakamori M, Imoto K, Wanifuchi H, Oka H, Oba A, Ikenaka K & Kurosaki T (1998). Differential distribution of TRP Ca^{2+} channel isoforms in mouse brain. *Neuroreport* **9**, 507-515

Okada T, Inoue R, Yamazaki K, Maeda A, Kurosaki T, Yamakuni T, Tanaka I, Shimizu S, Ikenaka K, Imoto K & Mori Y (1999). Molecular and functional characterization of a novel mouse transient recepotr potential protein homologue TRP7. *J Biol Chem* **274**, 27359-27370

Okada T, Shimizu S, Wakamori M, Maeda A, Kurosaki T, Takada N, Imoto K & Mori Y (1998). Molecular cloning and functional characterization of a novel

receptor-activated TRP Ca^{2+} channel from mouse brain. *J Biol Chem* **273**, 10279-10287

Pacaud P & Bolton TB (1991). Relation between muscarinic receptor cationic current and internal calcium in guinea-pig jejunal smooth muscle cells. *J Physiol* **441**, 477-499

Rusnak F & Mertz P (2000). Calcineurin: Form and Function. *Physiol Rev* **80**, 1483-1521

Saimi Y & Kung C (2002). Calmodulin as an ion channel subunit. *Annu Rev Physiol* **64**, 289-311

Siemen D (1993). Nonselective cation channels. *In*: Nonselective Cation Channels. Pharmacology, Physiology and Biophysics. Eds. D Siemen & J Hescheler, Birkhaeuser, Basel/Boston/Berlin

Shi J, Inoue R, Mori E, Mori Y & Ito Y (2003). Contrasting nature of calcium regulation via calmodulin (CaM) for two murine transient receptor potential protein homologues TRPC6 and TRPC7. *J Pharmacol Sci* **91** (sup I), 95P

Singh BB, Liu X, Tang J, Zhu MX & Ambudkar IS (2002). Calmodulin regulates Ca^{2+}-dependent feedback inhibition of store-operated Ca^{2+} influx by interaction with a site in the C terminus of TrpC1. *Mol Cell* **9**, 739-750

Strübing C, Krapivinsky G, Krapivinsky L & Clapham DE. (2003). Formation of novel TRPC channels by complex subunit interactions in embryonic brain. *J Biol Chem* **278**, 39014-39019

Tang J, Lin Y, Zhang Z, Tikunova S, Birnbaumer L & Zhu MX (2001). Identification of

common binding sites for calmodulin and inositol 1,4,5-trisphosphate receptors on the carboxyl termini of Trp channels. *J Biol Chem* **276**, 21303-21310

Trebak M, Vazquez G, Bird G St J & Putney JW Jr (2003). The TRPC3/6/7 subfamily of cation channels. *Cell Calcium* **33**, 451-461

Vaca L & Sampieri A (2002). Calmodulin modulates the delay period between release of calcium from internal stores and activation of calcium influx via endogenous TRP1 channels. *J Biol Chem* **277**, 42178-42187

Welsh DG, Morielli AD, Nelson MT & Brayden JE (2002). Transient receptor potential channels regulate myogenic tone of resistance arteries. *Circ Res* **90**, 248-250

Yamada H, Wakamori M, Hara Y, Takahashi Y, Konishi K, Imoto K & Mori Y (2000). Spontaneous single-channel activity of neuronal TRP5 channel recombinantly expressed in HEK293 cells. *Neurosci Lett* **285**, 111-114

Zhang Z, Tang J, Tikunova S, Johnson JD, Chen Z, Qin N, Dietrich A, Stefani E., Birnbaumer L & Zhu MX (2001). Activation of Trp3 by inositol 1,4,5-trisphosphate receptors through displacement of inhibitory calmodulin from a common binding domain. *Proc Natl Acad Sci USA*. **98**, 3168-3173

Zholos AV, Tsvilovskyy VV & Bolton TB (2003). Muscarinic cholinergic excitation of smooth muscle: signal transduction and single cationic channel properties. *Neurophysiol* **35** (3/4), 311-329.

Zitt C, Obukhov AG., Strübing C, Zobel A, Kalkbrenner F, Lückhoff A & Schultz G. (1997). Expression of TRPC3 in chinese hamster ovary cells results in calcium-activated cation currents not related to store depletion. *J Cell Biol* **138**,

1333-1341

Legend to Figures

Fig. 1 Acceleration of activation and inactivation time courses of murine TRPC6 currents by extracellular Ca^{2+} (Ca^{2+}_o). Holding potential: -60mV. A; typical traces for CCh (100μM)-evoked TRPC6 currents (I_{TRPC6}) in the presence (black, solid) and absence (gray, dotted) of 1mM Ca^{2+} in the bath, recorded from the same cell with nystatin-perforated recording. B; summary of latency (τ_{10}; time spent for 10% activation of the peak from the onset of CCh application), activation time (τ_{10-90}; time spent for 10-90% activation of the peak), and inactivation time (τ_{90-50}; time spent for 90-50% of the peak in inactivation phase) of I_{TRPC6} with 0 and 1mM Ca^{2+} evaluated from the experiments as shown in A (n=12). Repeated application of CCh at short intervals (<5min) usually resulted in a rundown and slowed activation and deactivation of I_{TRPC6}. To minimize the errors arising from this problem, I_{TRPC6} was activated at an interval of 10min, which recovered the second response to CCh to 0.82±0.09 of the first one (n=9; evaluated in Ca^{2+}-free external solution), and the response in the presence of Ca^{2+}_o was taken on the second application of CCh. C &D; I_{TRPC6} was first activated in the absence of Ca^{2+}_o and then exposed to 1mM Ca^{2+}_o, under nystatin-perforated and conventional whole-cell (10BAPTA/4Ca-internal solution) voltage clamp, respectively. E; summary of the effects of Ca^{2+}_o (1mM) on I_{TRPC6} such as illustrated in C and D. Relative I_{TRPC6} amplitude (fold change) is calculated as the ratio of I_{TRPC6} amplitude just after to that before (no Ca^{2+} present) application of Ca^{2+}_o. For slow Ca^{2+}_o-induced potentiation (#), I_{TRPC6} amplitude at the peak potentiation was normalized to that just before application of Ca^{2+}_o. Symbols "*-*" and "#" stand for the fast potentiation and slow potentiation,

respectively. n=5-8. '*' in B; P<0.05 with paired t-test. 'NS' in E denotes 'no statistical significance'.

Fig. 2 Biphasic effects of Ca^{2+}_o on I_{TRPC6} under strongly intracellular Ca^{2+} (Ca^{2+}_i)-buffering conditions. Recording conditions used were the same as in Fig. 1D. A&B; typical examples of I_{TRPC6} at varying $[Ca^{2+}]_o$ evoked by 100μM CCh (A) or OAG (B). C; relationships between $[Ca^{2+}]_o$ and relative I_{TRPC6} amplitude (fold change) under various conditions; 100μM CCh with $[Ca^{2+}]_i$=80nM (10mM BAPTA/4mMCa^{2+}, open circles) or 2μM (10mMBAPTA/9.5mMCa^{2+}, filled circles); 100μM OAG ($[Ca^{2+}]_i$=: 80nM, open triangles); 100μM GTPγS ($[Ca^{2+}]_i$: 80nM, open diamonds). n=5-12. D&E; typical examples of the effects of 1mM extracellular Sr^{2+} (D) and Ba^{2+} (E) on I_{TRPC6} evoked by 100μM CCh ($[Ca^{2+}]_i$: 80nM). F; relationships between relative I_{TRPC6} amplitude (fold change) and extracellular Ca^{2+}, Sr^{2+} or Ba^{2+} concentration. n=5-14. Curves in C and F are drawn according to the results of double Hill fitting (see the Methods), which gave the EC_{50} and IC_{50} values (mM): 0.44 and 3.56 (80nM), 0.42 and 3.61 (2μM), 0.38 and 4.27 (OAG), 0.41 and 3.54 (GTPγS) in C: 0.44 and 3.56 (Ca^{2+}), 0.84 and 7.44 (Sr^{2+}) in F, respectively.

Fig. 3 Potentiating and inhibitory effects of Ca^{2+}_o on single TRPC6 channels. A&B; O/O recording at -60mV. O/O membranes were sequentially exposed to CCh (100μM) and three different $[Ca^{2+}]_o$. A representative record (A) and the summary of five separate O/O experiments (B). Averaged NPo is plotted against $[Ca^{2+}]_o$. C; typical current-

voltage (I-V) relationships of I_{TRPC6} at different $[Ca^{2+}]_o$ (0, 1 or 10mM Ca^{2+} in the bath) evaluated from the same cell. D-F; C/A recording. Transmembrane potential was zeroed by high K^+ external solution. Typical examples of single CCh-activated TRPC6 channels at two different Ca^{2+} concentrations in the pipette (i.e. $[Ca^{2+}]_o$=1, 10mM) and membrane potentials (-100, 100mV) (D), and I-V relationships (E) and $[Ca^{2+}]_o$-dependence of NPo (F) of CCh-activated TRPC6 channels. n=5. In E, numerals indicate the unitary conductances evaluated by linear data fitting between -100 and 20mV (solid lines). *, **; P<0.05, 0.01 with paired t-test (in B) or ANOVA and pooled variance t-test (in F).

Fig.4 Inhibitory effects of $Ca^{2+}{}_o$ on I_{TRPC7} and single TRPC7 channels. A; typical examples of $Ca^{2+}{}_o$-induced inhibition of I_{TRPC7} recorded at -60mV, with nystatin-perforated (upper panel) or conventional whole-cell (10BAPTA/4Ca-internal solution: lower panel) recordings. In the latter, GTPγS (100μM) was included in a patch pipette. B; relationships between $[Ca^{2+}]_o$ and relative I_{TRPC7} amplitude (fold change induced by $Ca^{2+}{}_o$) under various conditions. Different activators (100μM CCh, OAG and GTPγS) and different modes of voltage-clamp (nystatin-perforated and conventional whole-cell recording with either 10BAPTA/4Ca- or 0.1EGTA-internal solution) were tested. * indicates P<0.05 with unpaired t-test for open vs. filled circles. Curves are drawn according to the results of single Hill fitting (see the Methods). n=5-10. C; typical I-V relationships for I_{TRPC7} obtained just before (Ca^{2+}-free) and after the addition of 1mM $Ca^{2+}{}_o$. D-F; C/A recording. Typical examples of single

CCh-activated TRPC7 channels at $[Ca^{2+}]_o$ of 0.1, 1 or 10mM and membrane potentials of -100 or 100mV (D), and I-V relationships (E) and $[Ca^{2+}]_o$-dependence of NPo (F) of CCh-activated TRPC7 channels. n=5. Solid lines and the meaning of numerals in E are the same as in Fig.3E. *,**; P<0.05, P<0.01 with ANOVA and pooled variance t-test.

Fig. 5 Essential requirement of CaM-kinase II-mediated phosphorylation for TRPC6 channel activation. Bath: 1mM Ca^{2+}-containing external solution. A; relationship between $[Ca^{2+}]_i$ and CCh (100μM)-evoked I_{TRPC6} density. n=5-19. B; typical examples of I_{TRPC6} recorded from cells coexpressing Ca^{2+}-insensitive mutant calmodulin (mutCaM: nystatin-perforated recording: top trace) and those intracellularly perfused (>5min; whole-cell: $[Ca^{2+}]_i$: 80nM; 10mM BAPTA/4mM Ca^{2+}) with 10μM CaM-kinase inhibitory peptide (middle trace) or MLCK inhibitory peptide (bottom trace). C; effects of calmidazolium (CMZ; 3μM) pretreatment or mutCaM coexpression on I_{TRPC6} evoked by 100μM CCh, OAG or GTPγS. n=5-15. D; effects of kinase and phosphatase inhibitors on I_{TRPC6} evoked by 100μM CCh or OAG.. Whole-cell recording ($[Ca^{2+}]_i$: 80nM). n=7-17. *,**; P<0.05, 0.01 with unpaired t-test (C: rightmost two columns in D) and with ANOVA and pooled variance t-test (the other columns in D: control is hatched).

Fig.6 CaM-mediated inhibition of I_{TRPC7}.

Bath: Ca^{2+}-free external solution. A; relationship between $[Ca^{2+}]_i$ and spontaneously activated (I_{spont}) or CCh (100μM)-evoked (I_{CCh}) I_{TRPC7}. n=8-14. Whole-cell recording.

B; a typical example of I_{TRPC7} recorded from a mutCaM-coexpressing cell under nystatin-perforated voltage clamp. C&D; CMZ pretreatment (3μM) or mutCaM coexpression enhances the density (C) and relieves Ca^{2+}_o (1mM)-induced inhibition (D) of I_{TRPC7}. Nystatin-perforated recording. n=7-20. E; ineffectiveness of inhibitors for MLCK, CaMKII and calcineurin for I_{TRPC7}. n=5-8. *,**: P<0.05, 0.01 with ANOVA and pooled variance t-test.

Fig.7 Differential dependence of single TRPC6 and TRPC7 channels on Ca^{2+}_i and CaM. I/O recording at -60mV. A & B, typical traces (lower panels) and corresponding NPo vs. time plots (upper panels) for CCh-activated TRPC7 (A) and TRPC6 (B) channels at different $[Ca^{2+}]_i$. Numerals and arrows indicate the value of $[Ca^{2+}]_i$ (in micromolar) and the timing of solution change, respectively. C & D; effects of CMZ on CCh-activated TRPC7 (C) and TRPC6 (D) channels. NPo vs. time plots. CMZ (3μM) was applied in C/A mode, and then patch membranes were excised (I/O mode). E & F; NPo-$[Ca^{2+}]_i$ relationships (I/O mode) for CCh-activated TRPC7 and TRPC6 channels, without (open circles) or with CMZ (3mM) treatment (filled circles) or mutCaM coexpression (open triangles). n=5-9. * indicates P<0.05 with pooled variance t-test for filled circle or open triangle vs. open circle at the same $[Ca^{2+}]_i$ (control).

Fig.8 Intracellular IP_3 differentially affect single TRPC7 and TRPC6 channel activities. A; typical trace (lower panel) and corresponding NPo vs. time plot (upper panel) for CCh-activated TRPC7 channel activities at two different $[Ca^{2+}]_i$ values

(<10nM and 0.11μM) with IP_3 (10μM) or wild-type CaM (1μM). I/O recording at -60mV. B; summary of the effects of Ca^{2+}_i, IP_3 (10μM) or CaM (1μM) on single TRPC7 and TRPC6 channel activities evaluated from experiments such as shown in A. n=5-8. C; typical examples of OAG (100μM)-induced I_{TRPC6} at -60mV with (lower panel) or without (upper panel) a subthreshold activating concentration of CCh (0.5μM). D; summary for the effects of intracellular IP_3 (10μM; added in the pipette) or a subthreshold concentration of CCh (0.5μM) on I_{TRPC6} and I_{TRPC7}. n=5-7. In C and D, bath and pipette contained 1mM Ca^{2+}-containing external and 0.1EGTA-internal solutions, respectively. *: P<0.05 with unpaired t-test or ANOVA and pooled variance t-test.

Fig.9 PKC mediates inactivation of TRPC6 and TRPC7 channels. A; representative records of CCh-evoked I_{TRPC6} with or without PKC inhibitory peptide [PKC-$IP_{(19-36)}$, 5μM] in the pipette. B; effects of PKC inhibitors on the inactivation time of I_{TRPC6} (τ_{90-50}; see Fig.1 legend); control (0.1EGTA-internal solution): pretreatment with calphostin C (500nM, 5min, middle): intracellular perfusion of PKC-$IP_{(19-36)}$ (5μM, 5min, right). n=7-12. Recording conditions in A and B were the same as in Fig.8C and D. C; effects of PKC inhibitors and activators on I_{TRPC6} or I_{TRPC7} density at two different $[Ca^{2+}]_i$ levels. n=5-12. *,**; P<0.05, 0.01 with unpaired t-test (in C) or ANOVA and pooled variance t-test (in B).

Supplementary Fig.1 Effects of Ca^{2+}_o on TRPC6/7 chimeras. Relative changes (fold change; see Fig.1 legend for definition) by 1mM Ca^{2+}_o in CCh-evoked currents recorded from six TRPC6/7 chimera-expressing cells (-60mV). Conventional whole-cell recording (10BAPTA/4Ca-internal solution). The inset depicts the structural arrangement of chimeras, where N, TM and C denote the amino-terminus, transmembrane domain and carboxy terminus of TRPC channels, respectively. n=5-10.

Supplementary Fig.2 C-terminus determines the pattern of Ca^{2+}_i response. I/O recording at -60mV. A; NPo-$[Ca^{2+}]_i$ relationships for two TRPC6/7 chimeras T667 (n=6) and T776 (n=10). B; NPo-$[Ca^{2+}]_i$ relationships for T667 with or without mutCaM coexpression. n=5. C; effects of mutCaM coexpression on T776 activity. $[Ca^{2+}]_i$: 0.11μM. n=5. D; typical NPo-time plot for CCh-activated T667 channels at different $[Ca^{2+}]_i$, with 10μM IP_3 or 1μM wild-type CaM. n=6. P value: unpaired t-test.

Supplementary Fig. 3 CLUSTALW amino acid alignments of putative TM5-6 linker region between TRPC7, 6 and 5 channels. '*', ':' and '.' denote the amino acid identity/similarity.

Figure 1

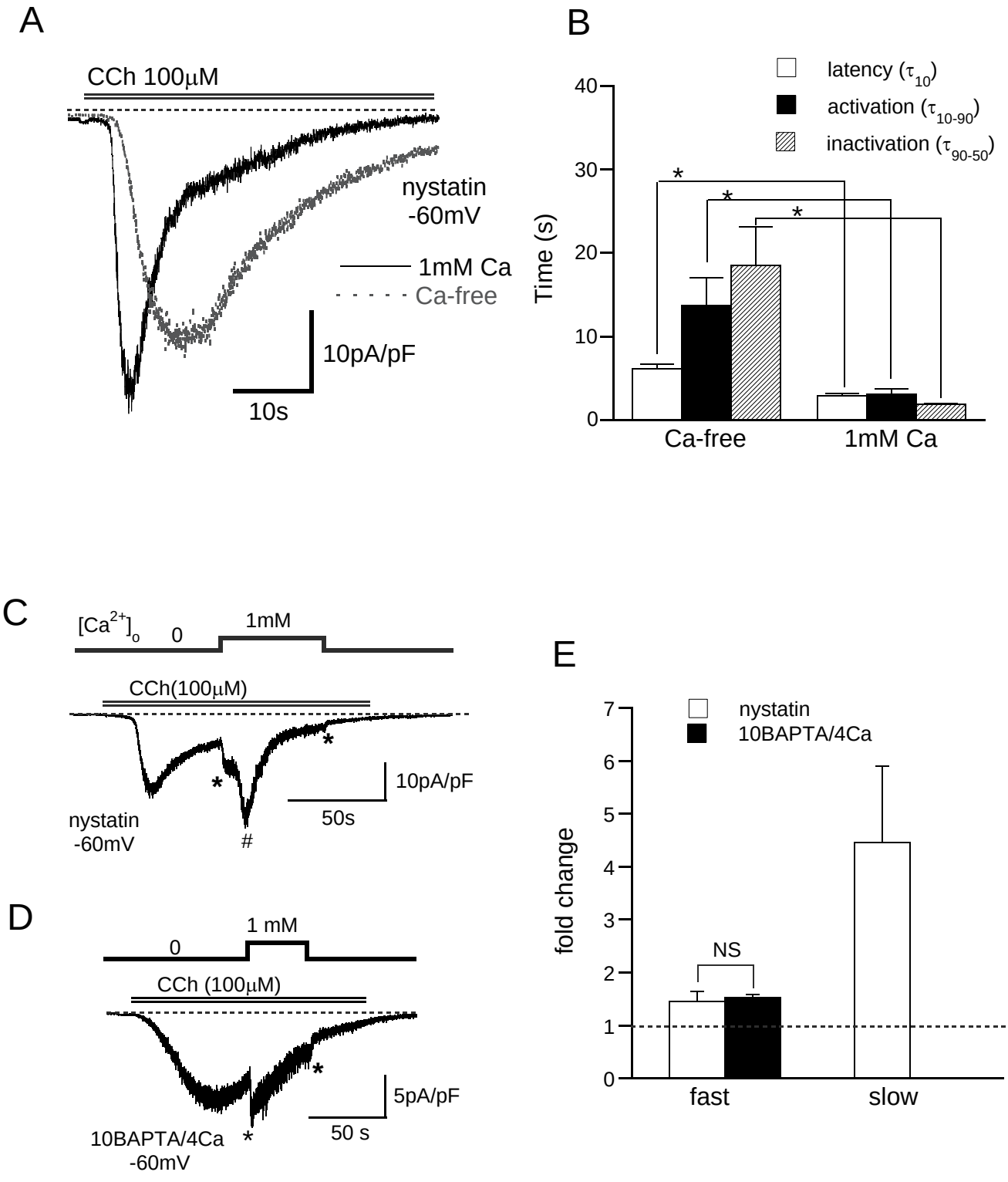
A
CCh 100μM
nystatin
-60mV
1mM Ca
Ca-free
10pA/pF
10s
B
latency (τ_{10})
activation (τ_{10-90})
inactivation (τ_{90-50})
Time (s)
40
30
20
10
0
*
*
*
Ca-free
1mM Ca
C
$[Ca^{2+}]_o$
0
1mM
CCh(100μM)
*
*
10pA/pF
50s
nystatin
-60mV
#
D
1 mM
0
CCh (100μM)
*
5pA/pF
50 s
10BAPTA/4Ca
-60mV
*
E
nystatin
10BAPTA/4Ca
fold change
7
6
5
4
3
2
1
0
NS
fast
slow

Figure 2

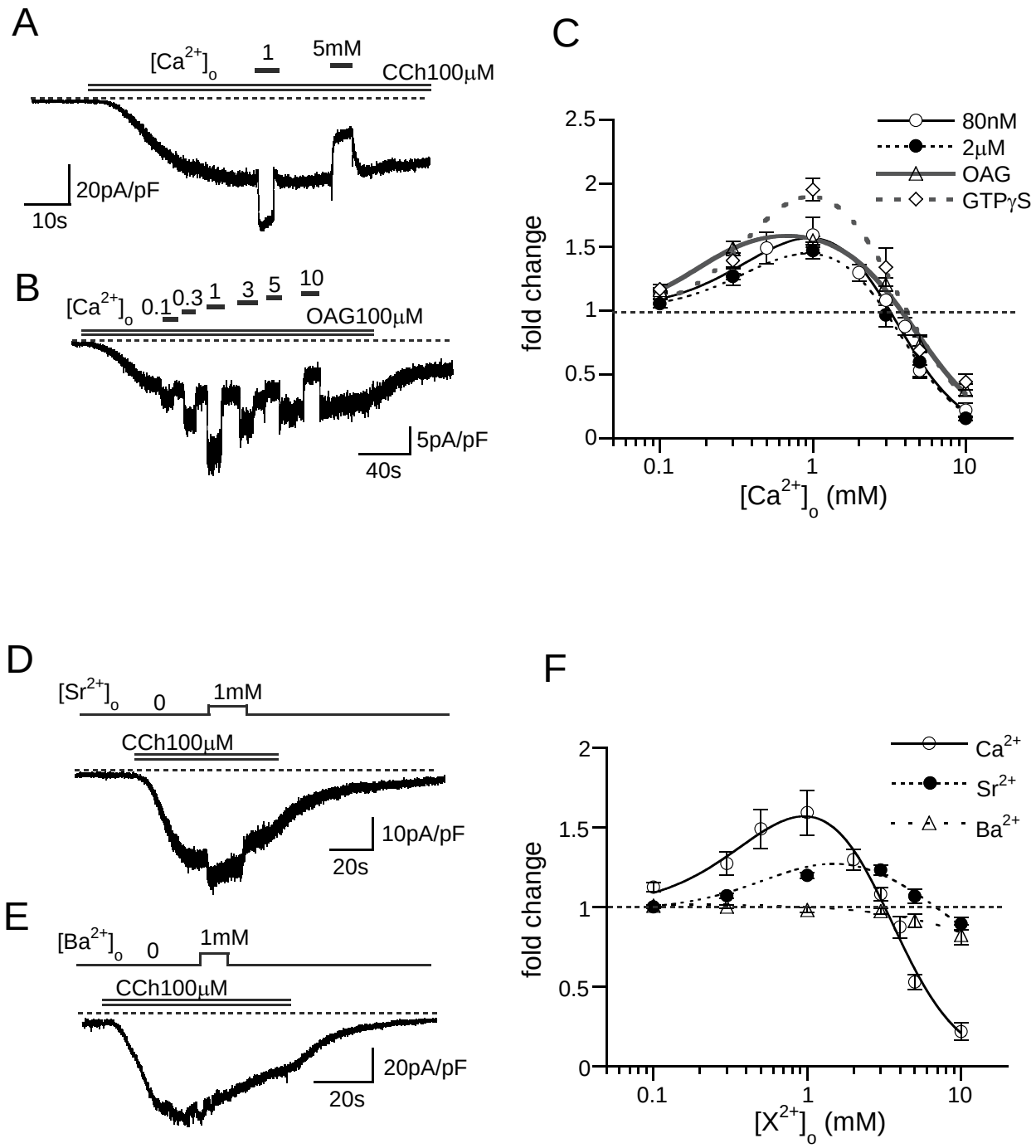
A
[Ca2+]o
1
5mM
CCh100μM
20pA/pF
10s
B
[Ca2+]o 0.1 0.3 1 3 5 10
OAG100μM
5pA/pF
40s
C
80nM
2μM
OAG
GTPγS
fold change
[Ca2+]o (mM)
D
[Sr2+]o
0
1mM
CCh100μM
10pA/pF
20s
E
[Ba2+]o
0
1mM
CCh100μM
20pA/pF
20s
F
Ca2+
Sr2+
Ba2+
fold change
[X2+]o (mM)

Figure 3

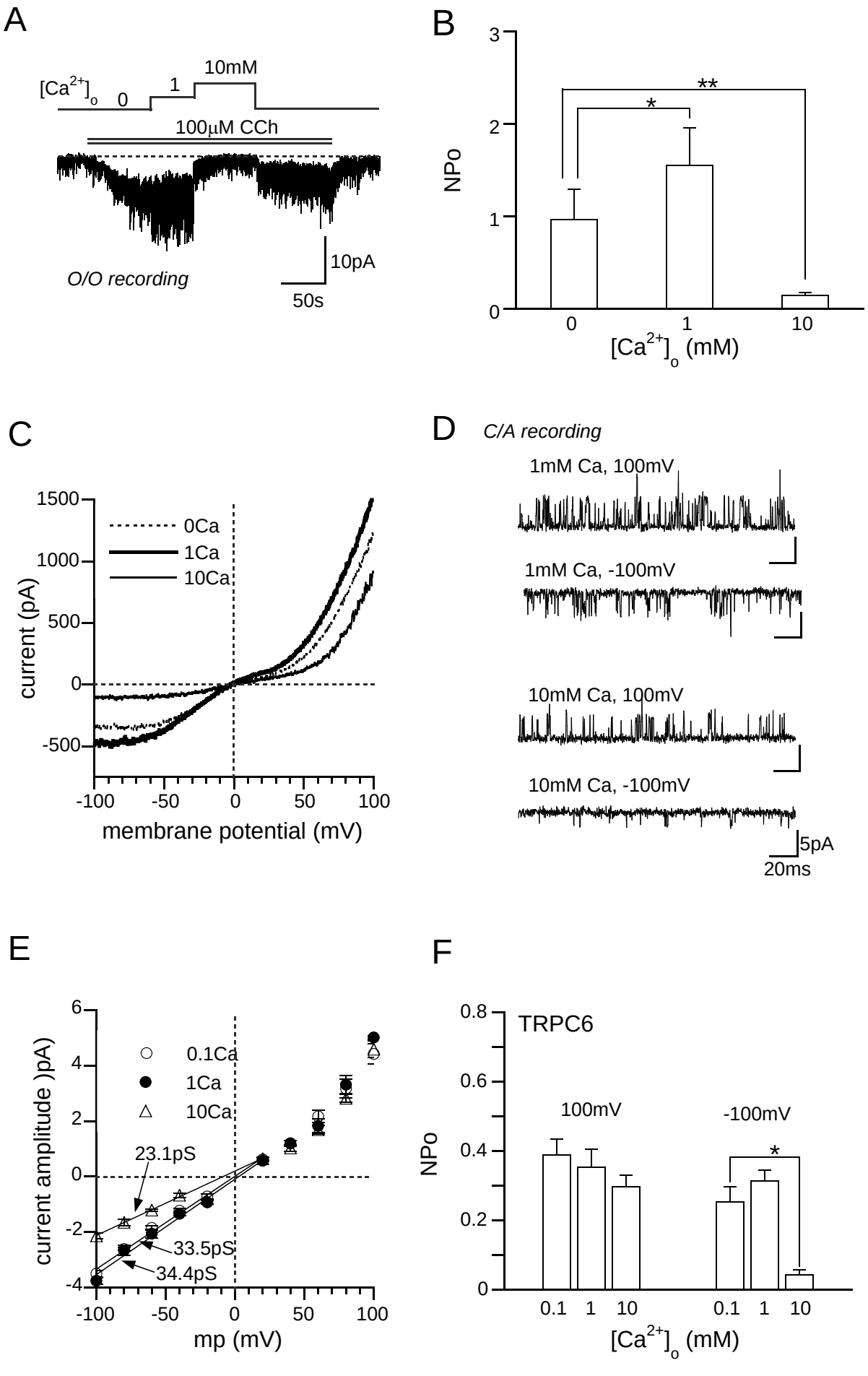
A
[Ca2+]o
0
1
10mM
100μM CCh
10pA
50s
O/O recording
B
NPo
3
2
1
0
*
**
0
1
10
[Ca2+]o (mM)
C
1500
1000
500
0
-500
current (pA)
0Ca
1Ca
10Ca
-100
-50
0
50
100
membrane potential (mV)
D
C/A recording
1mM Ca, 100mV
1mM Ca, -100mV
10mM Ca, 100mV
10mM Ca, -100mV
5pA
20ms
E
6
4
2
0
-2
-4
current amplitude)pA)
0.1Ca
1Ca
10Ca
23.1pS
33.5pS
34.4pS
-100
-50
0
50
100
mp (mV)
F
TRPC6
0.8
0.6
0.4
0.2
0
NPo
100mV
-100mV
*
0.1
1
10
0.1
1
10
[Ca2+]o (mM)

Figure 4

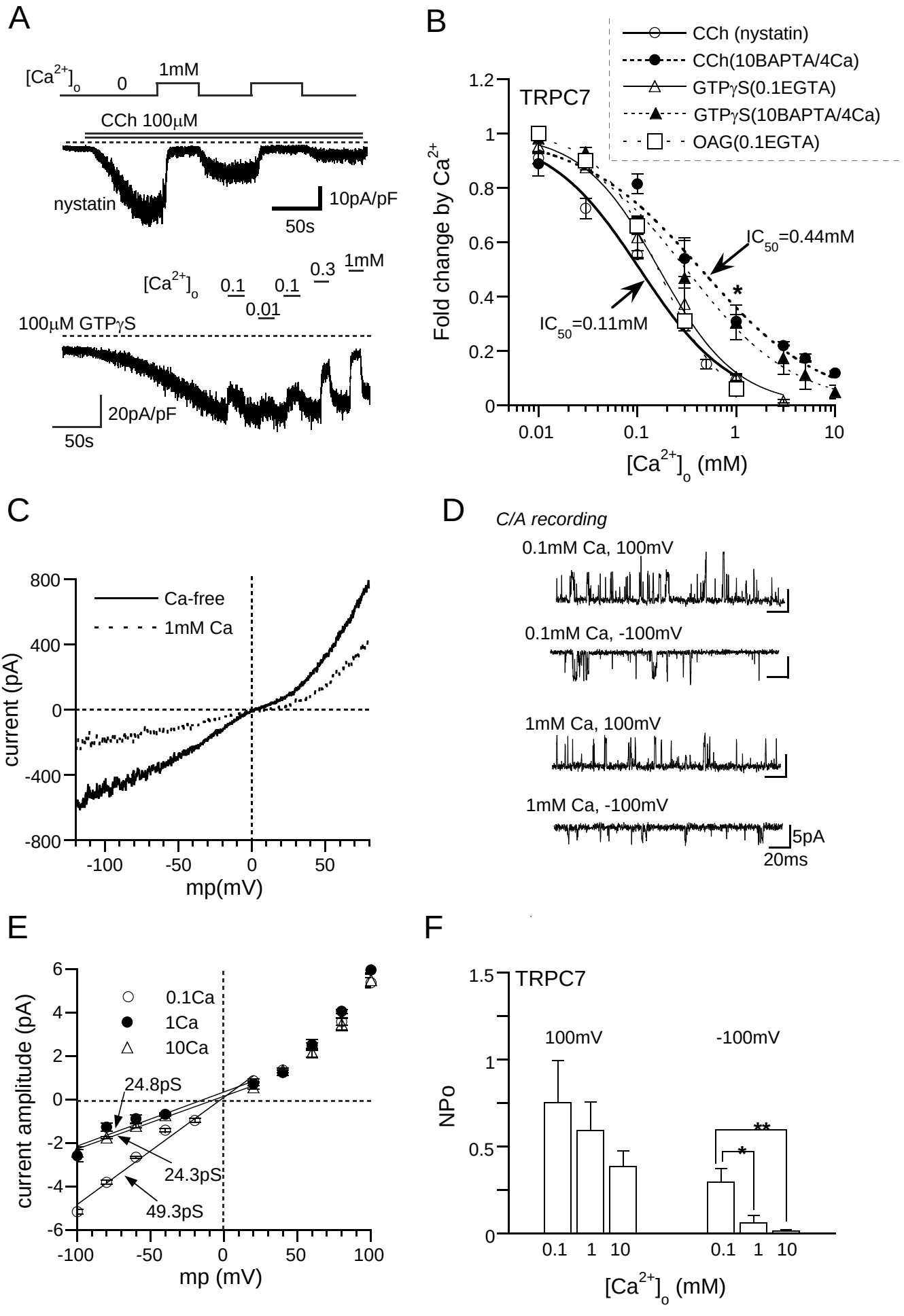
A
[Ca2+]o
0
1mM
CCh 100μM
nystatin
10pA/pF
50s
[Ca2+]o
0.1
0.1
0.3
1mM
0.01
100μM GTPγS
20pA/pF
50s
B
CCh (nystatin)
CCh(10BAPTA/4Ca)
GTPγS(0.1EGTA)
GTPγS(10BAPTA/4Ca)
OAG(0.1EGTA)
TRPC7
Fold change by Ca2+
IC50=0.44mM
IC50=0.11mM
[Ca2+]o (mM)
C
Ca-free
1mM Ca
current (pA)
mp(mV)
D
C/A recording
0.1mM Ca, 100mV
0.1mM Ca, -100mV
1mM Ca, 100mV
1mM Ca, -100mV
5pA
20ms
E
0.1Ca
1Ca
10Ca
24.8pS
24.3pS
49.3pS
current amplitude (pA)
mp (mV)
F
TRPC7
100mV
-100mV
NPo
[Ca2+]o (mM)

Figure 5

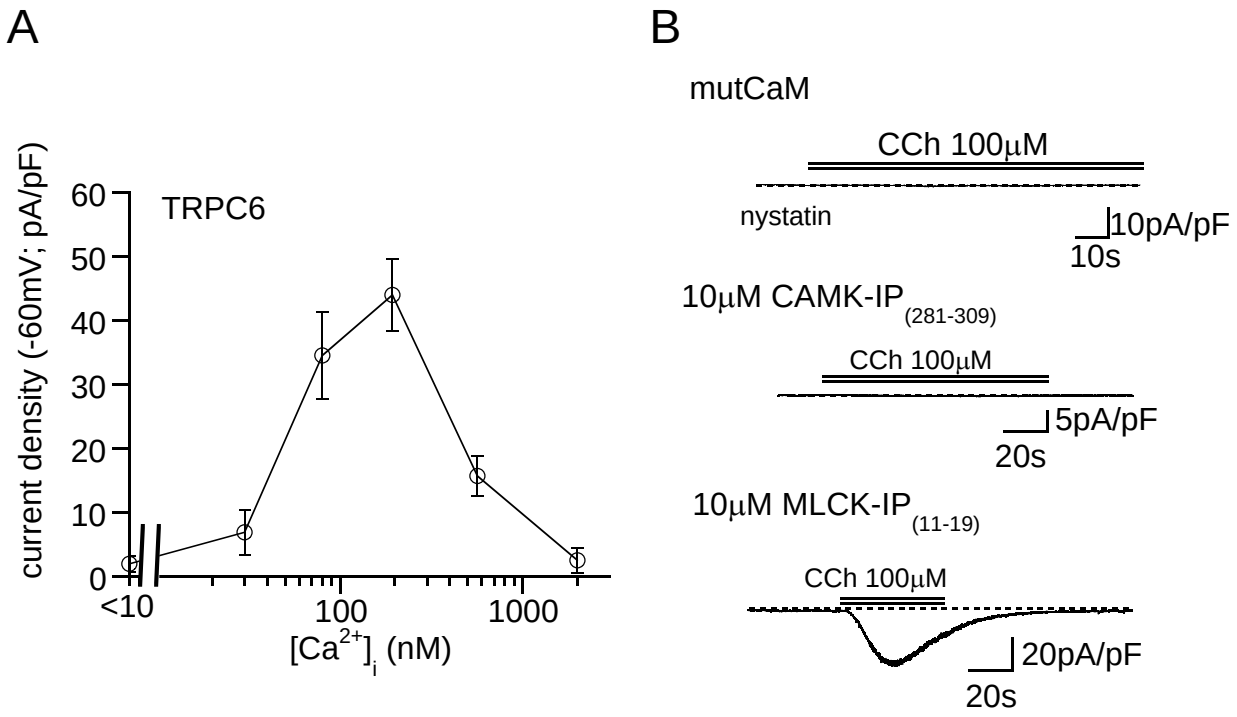
A
TRPC6
current density (-60mV; pA/pF)
60
50
40
30
20
10
0
<10
100
1000
[Ca2+]i (nM)
B
mutCaM
CCh 100μM
nystatin
10pA/pF
10s
10μM CAMK-IP(281-309)
CCh 100μM
5pA/pF
20s
10μM MLCK-IP(11-19)
CCh 100μM
20pA/pF
20s

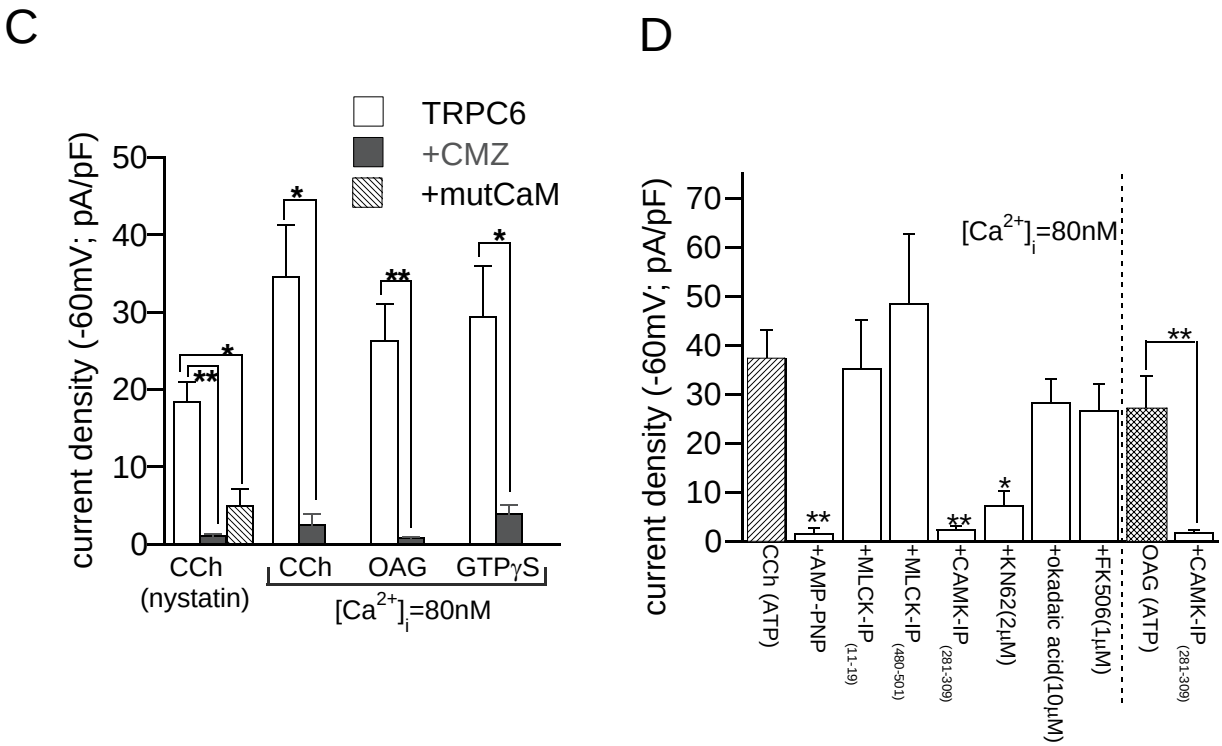
C
TRPC6
+CMZ
+mutCaM
current density (-60mV; pA/pF)
50
40
30
20
10
0
CCh (nystatin)
CCh
OAG
GTPγS
[Ca2+]i=80nM
D
current density (-60mV; pA/pF)
70
60
50
40
30
20
10
0
[Ca2+]i=80nM
CCh (ATP)
+AMP-PNP
+MLCK-IP(11-19)
+MLCK-IP(480-501)
+CAMK-IP(281-309)
+KN62(2μM)
+okadaic acid(10μM)
+FK506(1μM)
OAG (ATP)
+CAMK-IP(281-309)

Figure 6

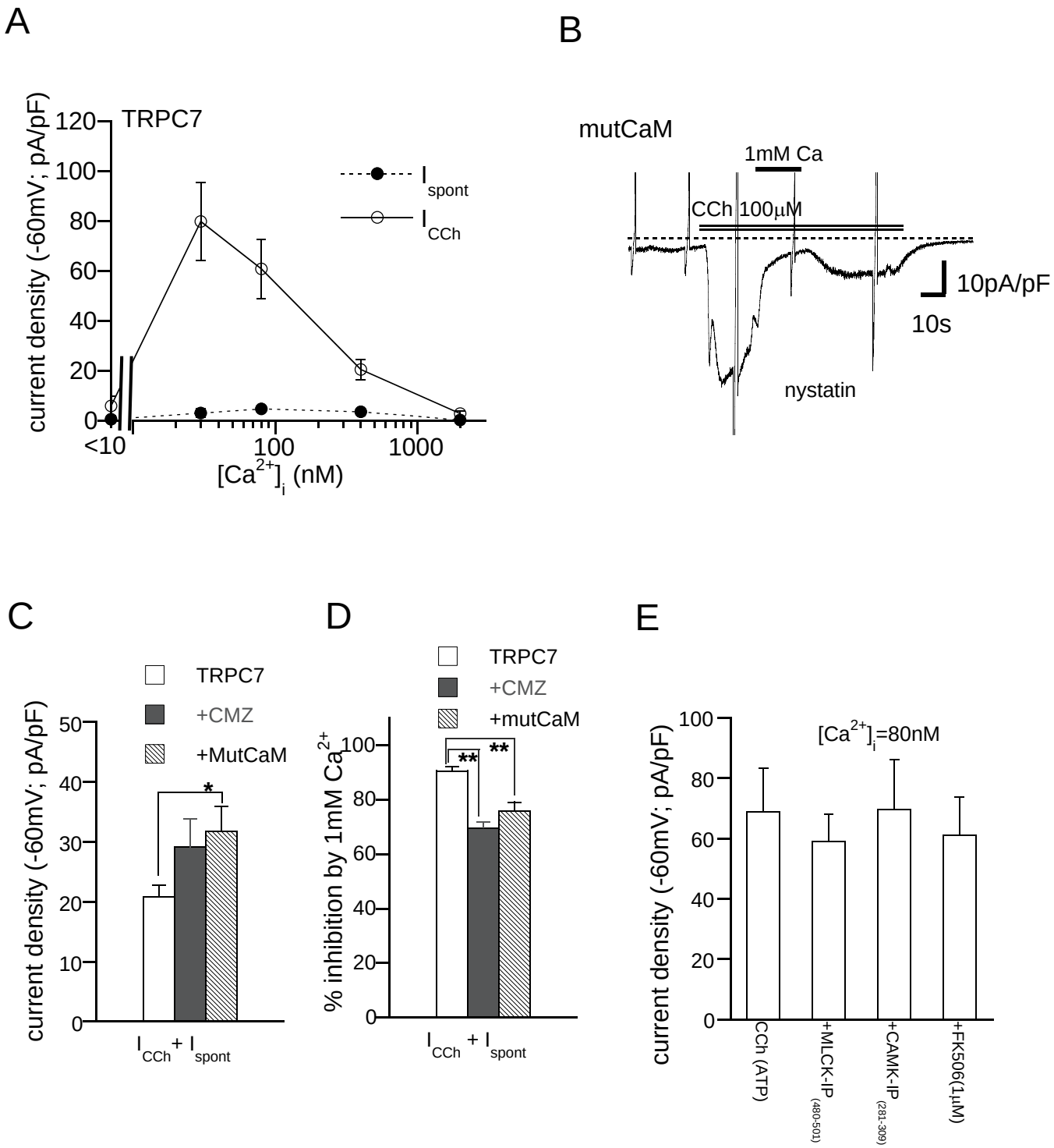
A
TRPC7
current density (-60mV; pA/pF)
120
100
80
60
40
20
0
<10
100
1000
[Ca2+]i (nM)
Ispont
ICCh
B
mutCaM
1mM Ca
CCh 100μM
10pA/pF
10s
nystatin
C
TRPC7
+CMZ
+MutCaM
current density (-60mV; pA/pF)
50
40
30
20
10
0
*
ICCh + Ispont
D
TRPC7
+CMZ
+mutCaM
% inhibition by 1mM Ca2+
100
80
60
40
20
0
**
**
ICCh + Ispont
E
[Ca2+]i=80nM
current density (-60mV; pA/pF)
100
80
60
40
20
0
CCh (ATP)
+MLCK-IP (480-501)
+CAMK-IP (281-309)
+FK506(1μM)

Figure 7

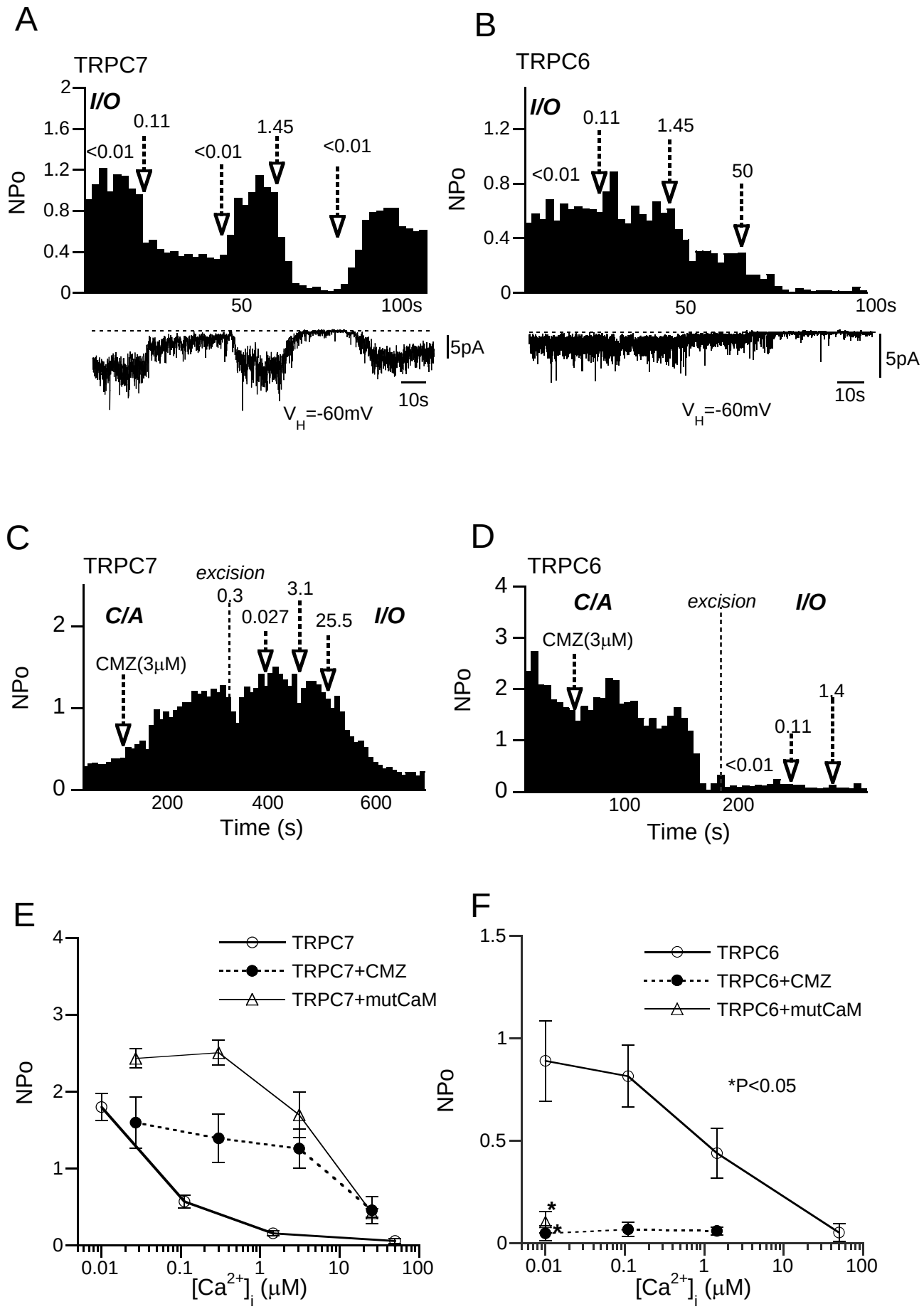
A
TRPC7
I/O
0.11
1.45
<0.01
<0.01
<0.01
NPo
50
100s
5pA
10s
V_H=-60mV
B
TRPC6
I/O
0.11
1.45
50
<0.01
NPo
50
100s
5pA
10s
V_H=-60mV
C
TRPC7
excision
0.3
3.1
C/A
0.027
25.5
I/O
CMZ(3μM)
NPo
Time (s)
D
TRPC6
C/A
excision
I/O
CMZ(3μM)
1.4
0.11
<0.01
NPo
Time (s)
E
TRPC7
TRPC7+CMZ
TRPC7+mutCaM
NPo
[Ca2+]i (μM)
F
TRPC6
TRPC6+CMZ
TRPC6+mutCaM
*P<0.05
NPo
[Ca2+]i (μM)

Figure 8

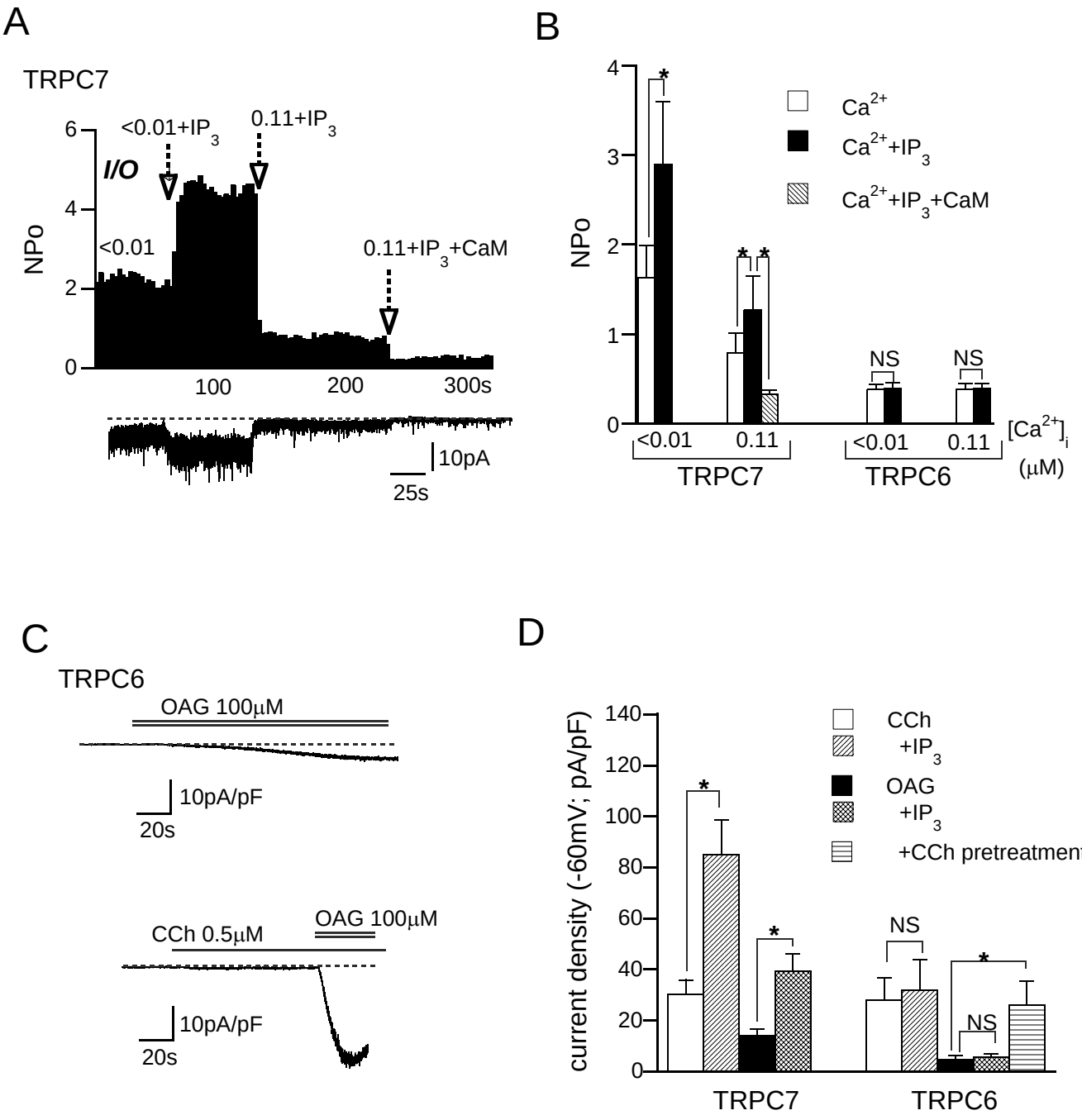
A
TRPC7
<0.01+IP3
0.11+IP3
I/O
<0.01
0.11+IP3+CaM
NPo
100
200
300s
10pA
25s
B
Ca2+
Ca2+ +IP3
Ca2+ +IP3 +CaM
NPo
NS
NS
<0.01
0.11
<0.01
0.11
[Ca2+]i
(μM)
TRPC7
TRPC6
C
TRPC6
OAG 100μM
10pA/pF
20s
CCh 0.5μM
OAG 100μM
10pA/pF
20s
D
CCh
+IP3
OAG
+IP3
+CCh pretreatment
current density (-60mV; pA/pF)
NS
NS
TRPC7
TRPC6

Figure 9

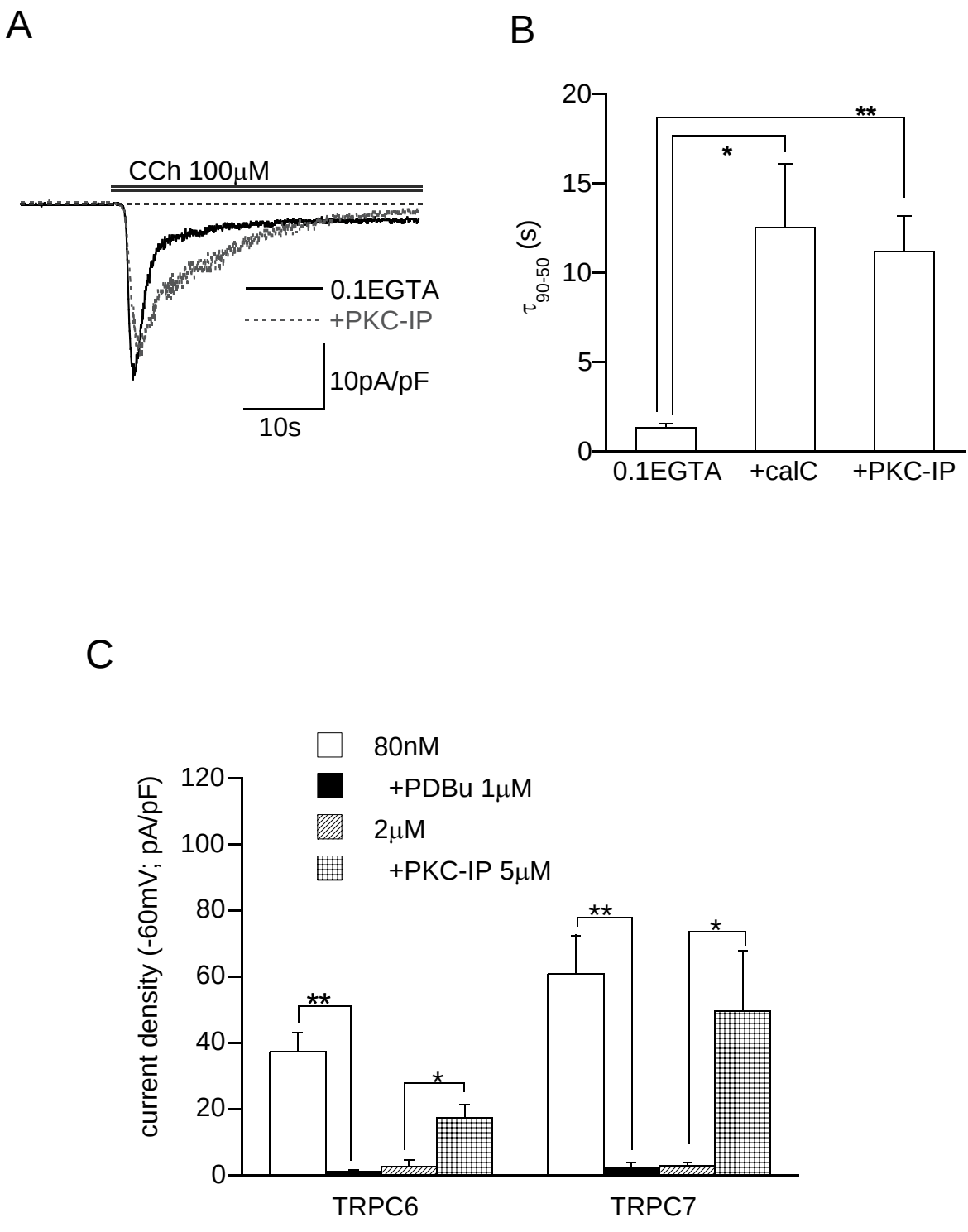
A
CCh 100μM
0.1EGTA
+PKC-IP
10pA/pF
10s
B
τ_{90-50} (s)
20
15
10
5
0
**
*
0.1EGTA
+calC
+PKC-IP
C
80nM
+PDBu 1μM
2μM
+PKC-IP 5μM
current density (-60mV; pA/pF)
120
100
80
60
40
20
0
**
*
**
*
TRPC6
TRPC7